REACTOR ACCELERATOR COUPLING EXPERIMENTS:

A FEASIBILITY STUDY

A Thesis

by

TARAKNATH WODDI VENKAT KRISHNA

Submitted to the Office of Graduate Studies of
Texas A&M University
in partial fulfillment of the requirements for the degree of

MASTER OF SCIENCE

May 2005

Major Subject: Nuclear Engineering

REACTOR ACCELERATOR COUPLING EXPERIMENTS:

A FEASIBILITY STUDY

A Thesis

by

TARAKNATH WODDI VENKAT KRISHNA

Submitted to the Office of Graduate Studies of
Texas A&M University
in partial fulfillment of the requirements for the degree of

MASTER OF SCIENCE

Approved as to style and content by:

William S. Charlton (Chair of Committee)	Marvin L. Adams (Member)
Rabi Mahapatra (Member)	Ronald J. Ellis (Member)
William E. Burchill (Head of Department)	

May 2005

Major Subject: Nuclear Engineering

ABSTRACT

Reactor Accelerator Coupling Experiments: A Feasibility Study. (May 2005)

Taraknath Woddi Venkat Krishna, B. Tech.,

Orissa University of Agriculture and Technology

Chair of Advisory Committee: Dr. William S. Charlton

The Reactor Accelerator Coupling Experiments (RACE) are a set of neutron source driven subcritical experiments under temperature feedback conditions. These experiments will involve coupling an accelerator driven neutron source to a TRIGA reactor system in a subcritical configuration. The accelerator source will consist of a 40 MeV electron linear accelerator (LINAC) and a heavy metal target. The electrons from the accelerator produce bremsstrahlung radiation in the target which in turn produces a source of neutrons via photonuclear reactions. The available core at the The University of Texas at Austin (UT) with standard TRIGA fuel will be used to carry out these studies.

The primary objective of this thesis was to study the feasibility of RACE especially with respect to the heat generation rates capable of placing the reactor in a temperature feedback regime. First, the accelerator target (or neutron source) was optimized for size, shape, and type of material to be used. Analyses were then performed for several arrangements of this target in the UT TRIGA reactor. One of these arrangements was found to provide heat generation rates well into the temperature feedback regime of the fuel. Lastly, a multi-target system [named the Texas

Transmutation System (TTS)] was designed to allow for more detailed accelerator driven systems (ADS) studies. It was shown that this system would allow for operation over a wide-range of subcriticalities and with a wide-range of heat loads. Thus, the feasibility for these experiments has been proven, and it is recommended that continued study and implementation of these experiments be performed.

ACKNOWLEDGEMENTS

This thesis would not have been possible without Dr. William Charlton giving me the opportunity to work on his project. It was because of his faith and support that I could reach a point to where my contribution to the efforts of ADS has been acknowledged.

I convey my sincere gratitude to all my committee members: Dr. Marvin Adams, Dr. Ronald Ellis and Dr. Rabi Mahapatra for sparing their precious time and giving me useful suggestions.

I would take this opportunity to thank Dr. Hart, Dr. Reece and Dr. Ragusa for creating an academic acumen in me and for providing the required technical skill set to attain the goals of this research.

No honors are complete without the blessings and help of family and friends. My mom (Basanti), my dad (Pattabhiram), my wife (Divya), my sister (Jeanie) and brother in law (Tanuj) were the pillars of confidence during hard times. My friends Julien Partouche, David Oertli, David Burk, Kaydee Kohlhepp and Alexander Pasciak were the spring board for getting me over the research hurdles.

TABLE OF CONTENTS

Page

ABSTRACT iii

ACKNOWLEDGEMENTS v

TABLE OF CONTENTS vi

LIST OF TABLES viii

LIST OF FIGURES ix

I. INTRODUCTION 1

I.A. RACE Overview 4
I.B. Theory 5
I.C. Previous Work 7
I.C.1. Background 7
I.C.2. Muse Experiments 9
I.C.3. TRADE Experiments 10
I.D. Project Overview 10

II. ACCELERATOR DRIVEN NEUTRON SOURCE DESIGN 11

II.A. Lead Target Optimization 12
II.A.1. MCNP Parameter Optimization 13
II.B. Tungsten Target Optimization 15
II.C. Tungsten-Copper Alloy Target Optimization 18
II.D. Target Cooling 19

III. ANALYSIS OF EXPERIMENTS USING UT NETL TRIGA REACTOR 20

III.A. Description of UT NETL 20
III.B. Analysis of Experimental Arrangements at UT NETL 22
III.B.1. Core Arrangement #1 23
III.B.2. Core Arrangement #2 26
III.B.3. Core Arrangement #3 28
III.B.4. Core Arrangement #4 31

Page

III.C. Optimal Core Configuration for UT-NETL RACE 34

IV. TEXAS TRANSMUTATION SYSTEM DESIGN 38

IV.A. History of TAMU NSC Reactor 38
IV.B. TTS Design Concept 40
IV.C. TTS Evaluation Results 42

V. CONCLUSIONS 48

REFERENCES 51

APPENDIX A 55

APPENDIX B 58

APPENDIX C 72

VITA 77

LIST OF TABLES

Page

Table I. Principal Design Characteristics of the UT-NETL Reactor 21

Table II. Heat Generation Rate for Lead Target in BP#5 24

Table III. Heat Generation Rate for Tungsten Target in BP#5 25

Table IV. Heat Generation Rate for Tungsten-Copper Target in BP#5 26

Table V. Heat Generation Rate for Lead Target in Core Arrangement #2 27

Table VI. Heat Generation Rate for Tungsten Target in Core Arrangement #2 28

TableVII. Heat Generation Rate for Tungsten-Copper Target in Core Arrangement #2 28

Table VIII. Heat Generation Rate for Lead Target in Core Arrangement #3 30

Table IX. Heat Generation Rate for Tungsten Target in Core Arrangement #3 30

TableX. Heat Generation Rate for Tungsten-Copper Target in Core Arrangement #3 30

Table XI. Heat Generation Rate for Tungsten-Copper Target in Core Arrangement #4 with the Target Located at Different Axial Heights 32

Table XII. Heat Generation Rate for Tungsten-Copper Target in Core Arrangement #4 with the Target Located at Different Axial Heights 34

Table XIII. Heat Generation Rate for TTS Design 41

LIST OF FIGURES

Page

Fig. 1. Exiting neutron current versus target radius for lead target. 12

Fig. 2. Exiting neutron current versus target length for lead target. 13

Fig. 3. Exiting neutron current versus target radius for tungsten target. 16

Fig. 4. Exiting neutron current versus target length for tungsten target. 16

Fig. 5. Exiting neutron current versus target radius for W-Cu target. 17

Fig. 6. Exiting neutron current versus target length for W-Cu target. 18

Fig. 7. Target with cooling jacket. 19

Fig. 8. UT-NETL TRIGA reactor under operation and cross sectional core layout. 22

Fig. 9. Screen capture of MCNP geometry for UT–NETL experiment with accelerator source in beam port # 5. 24

Fig. 10. Screen capture of MCNP geometry for UT–NETL experiment with accelerator source target at the center of the core. 27

Fig. 11. Screen capture of MCNP geometry for UT–NETL experiment with target at the center of the core and control rods one fuel element away. 29

Fig. 12. Screen capture of MCNP geometry for UT–NETL experiment with target along with jacket at the center of the core and rods two fuel element away. 32

Fig. 13. Screen capture of MCNP geometry for UT–NETL experiment with accelerator source target at core center with (a) cladding, (b) no cladding, and (c) no cladding and larger radius. 33

Fig. 14. Screen capture of axial view of the final design MCNP geometry for UT–NETL reactor accelerated coupled experiment. 35

Fig. 15. k_{eff} versus control rod positions. 36

Page

Fig. 16. Heat generation versus rod position. 36

Fig. 17. Heat generation versus k_{eff}. 37

Fig. 18. MCNP geometry of TTS TAMU with four target positions 41

Fig. 19. Heat generation in the four targets due to neutron reactions. 43

Fig. 20. Heat production in the four targets due to photon reactions. 44

Fig. 21. Total heat production in the four targets. 44

Fig. 22. Heat generation rate in fuel due to neutron reactions. 45

Fig. 23. Heat generation rate in the fuel due to photon reactions. 46

Fig. 24. Total heat generation rate in fuel. 46

I. INTRODUCTION

The quantity of spent fuel discharged from U.S. nuclear reactors will reach 87,000 tons by the time the existing U.S. nuclear plants reach the end of their license period. This discharged fuel contains 95% uranium (comparable to natural uranium), about 1-2% transuranic elements (principally plutonium), and 3% fission products and activation elements. Most fission products decay to stable nuclides within a few decades; however, a small number of nuclides (^{99}Tc and ^{129}I, for example) remain radioactive for many thousands of years and contribute to long-term repository waste management requirements. The amount of plutonium existing today is approximately 600 tons, and at the end of the license period for the current U.S. fleet of reactors it will reach 870 tons. The inventory of ^{99}Tc and ^{129}I will be 78.3 tons [1].

The radiotoxicity of spent nuclear fuel remains at a level above that of natural uranium for 200,000 years after discharge from a typical light water reactor [2]. The majority of the long-term radiotoxicity of spent nuclear fuel is due to the transuranic radionuclides. If both plutonium and americium are completely transmuted to stable or shorter-lived nuclides, the required lifetime of a geological repository can be drastically reduced. This transmutation can be performed via fission. The fission process would result in the generation of generally shorter-lived fission products and would produced useable energy.

This thesis follows the style of *Nuclear Technology*.

Current fast reactor designs would be able to transmute the plutonium via fission with a reasonable degree of efficiency; however, from a safety perspective, limits on the allowable concentration of minor actinides (i.e, neptunium, americium, and curium) in fissile fuel for critical reactor systems is about 5%. This is due primarily to the lower delayed neutron fraction and Doppler reactivity coefficient effects from these nuclides. Taking into account the large inventory of americium arising from the decay of ^{241}Pu presently being stored, it is of primary necessity that realistic transmuters for burning these minor actinides are developed. It has also been shown that critical fast reactor systems are not capable of transmuting the fission product waste from spent nuclear fuel [3]. This is due to the criticality limitation on neutron conservation in the system (i.e., one neutron from each fission chain must cause another fission to continue the self-sustaining chain reaction). There simply are not enough neutrons per fission available in a critical fast reactor to transmute plutonium, minor actinides, and fission products.

One system which may be capable of transmuting the plutonium, minor actinides, and fission product constituents of spent nuclear fuel is an accelerator driven system (ADS). An ADS consists of a subcritical array of fuel driven by an accelerator produced neutron source. Since the system is subcritical, there is no criticality limitation on the neutrons in the fission chain. Thus, if needed every neutron from the source per fission could be used to transmute materials.

The state of ADS research has advanced considerably in the last 15 years. A variety of ADS designs have been studied in the past [3-7], and a number of accelerator

driven neutron sources have been designed and built over the years (including fusion sources using D-T fusion, spallation neutron sources using a proton beam, and photoneutron sources using an electron accelerator). However, an ADS system of significant power has never been built and operated. The knowledge base relating the operational characteristics of these systems is virtually non-existent.

ADS has been studied for use in transmutation of nuclear waste, production of energy, tritium production, and incineration of weapons grade plutonium; however, the experimental research in this field is sparse. This is at least in part due to the high costs associated with most high-energy particle accelerators. In this regard, experimental research with ADS on the basis of lower energy accelerators is of great importance and could provide valuable prototyping data.

This thesis describes a set of experiments, named the Reactor Accelerator Coupled Experiments (RACE), which are being planned in Texas and will provide operational data for ADS operated at significant power levels and with reactivity feedback. These experiments will involve coupling an accelerator driven neutron source to a TRIGA reactor system in a subcritical configuration. The accelerator source will consist of an electron linear accelerator (LINAC) and a heavy metal target. The electrons from the accelerator produce Bremsstrahlung radiation in the target which in turn produces a source of neutrons via photonuclear reactions. Of principle interest in these experiments is to operate at a power level which would allow for observation of thermal feedback effects on the subcritical system (generally above 1-kW). In this work, the

feasibility of these experiments was studied especially with respect to the capability of the system to allow for operation in the thermal feedback regime of a TRIGA reactor.

I.A. RACE Overview

Both the University of Texas at Austin (UT) and Texas A & M University (TAMU) operate 1-MW TRIGA research reactors. These reactor systems use TRIGA reactor fuel which has been shown to have exceptional safety characteristics even under the most extreme transients. The RACE experiments will couple the accelerator source to these TRIGA reactors to study the operational characteristics of these ADS. The source of neutrons is expected to have strength on the order of 1×10^{13} n/s. These experiments are expected to allow for study of the following:

1. Behavior of an ADS at power levels between 1-20 kW and at various levels of subcriticality (ranging from k_{eff}=0.90 to k_{eff}=0.99)
2. Methods for level of subcriticality measurement at significant powers.
3. Reactivity control by various means including via neutron source importance variation.
4. Compensation of reactivity feedback with control rod adjustment or by altering the accelerator current.

The RACE project has four principle goals:

1. Produce an ADS demonstration with adjustable reactivity to demonstrate the ability to design, compute, and conduct ADS experiments and benchmark the ability to predict and analyze subcritical source-driven transients.

2. Provide ADS benchmark data for developing codes and methods for analyzing static and transient behavior.
3. Produce a teaching tool that can be used to educate the next generation of scientists and engineers in the operation and modeling of ADS and in advanced nuclear science.
4. Advance the state of knowledge of ADS transmutation

A neutron source will be built and tested at Idaho State University for this project. This neutron source will be coupled to the UT Nuclear Engineering Teaching Laboratory (NETL) 1-MW TRIGA Mark II research reactor to study static and transient operation characteristics.

After completion of the experiments at UT, the accelerator driven source will be moved to the Nuclear Science Center (NSC) at TAMU. A subcritical assembly composed of spent fuel discharged from the TAMU NSC TRIGA reactor will be designed and built for location in the NSC pool. The accelerator driven source will be inserted into the reactor and used to evaluate static and transient effects with the source in several internal locations in the core and with adjustable reactivities up to k_{eff} of 0.98.

I.B. Theory

As envisaged, ADS is a promising new concept for transmutation of long-lived nuclides from spent nuclear fuel. The principal system under study is the proton accelerator driven ADS. These proton accelerators are generally large scale facilities requiring large capital and operating costs. The RACE program will make use of a

smaller scale system with an electron LINAC driven neutron source. There are several advantages in using an electron beam rather than a proton beam including:

1. Electron accelerators are small and compact machines
2. Less costly to build and operate,
3. More dependable and safer to operate and
4. Considerably lower activation compared to proton machines.

The primary disadvantage is that the electron LINAC will produce much smaller neutron source strengths.

There are three main components of an ADS. These are: (1) a high-intensity accelerator, (2) an accelerator target which will produce neutrons, and (3) a transmuter (that is, a sub-critical reactor-like system containing the material to be transmuted). For the purposes of this work, we will neglect the development of the accelerator and assume that it will be provided. This thesis will focus on the target and transmuter.

When a particle beam from an accelerator hits a thick target of heavy elements (e.g., lead, tungsten, uranium, etc.), a large number of neutrons are obtained. In the case of a proton accelerator, these neutrons are produced via spallation reactions [8]. In the case of an electron accelerator, the electrons are slowed down in the target and emit Bremsstrahlung radiation. These high energy photons then lead to photoneutron reactions in the target. In both cases, most of the charged particles are slowed down and stopped inside the target or in its immediate vicinity due to the Coulomb interaction. The

neutrons however penetrate to the outer surface of the target and reach the surrounding subcritical core.

The external neutrons supplied by photoneutron reactions in the target sustain a constant power in the ADS via subcritical multiplication. The neutrons born in the target have energies ranging from "usual" fission energies (about 1 MeV) up to the energy of the incident charged particles from the accelerator. The neutrons born in the fuel have energies around 1 MeV. The total power in this system can then be adjusted by raising or lowering the current of the accelerator. The power in the ADS is directly dependent upon the power from the accelerator. If the accelerator power is removed, the ADS will shutdown (aside from any decay heat effects). Thus, under normal operating conditions, the ADS have inherent safety from transient effects. Transients in the system which do not increase criticality above k_{eff}=1 will always result in a linear response by the ADS (as opposed to an exponential response by a critical system). These inherent safety features make ADS an excellent option when transmuting actinides with lower delayed neutron fractions (like plutonium and americium).

I.C. Previous Work

I.C.1. Background

The first significant investigation of using a spallation system for high-level waste transmutation was the APEX project conducted at Brookhaven National Laboratory [9]. The design concept application was to transmutate ^{90}Sr and ^{137}Cs, dominate long-lived fission products of reactor spent fuel. The system consisted of a

1500 MeV proton accelerator operating at 300 mA impinging upon a flowing liquid lead target with a blanket of fertile material surrounding the target. The study concluded that the radioactivity of the spent fuel could be reduced by a factor of ten. The disadvantage of this study was there were no technical specifications provided for the target dimensions and operation of the flowing lead system.

Another study to transmutate actinides of reactor spent fuel was conducted by Nishida *et al.* [10]. The design concept was a 1500 MeV, 7.8 mA accelerator using a transuranic target with a liquid lead-bismuth eutectic (LBE) coolant to transmutate actinide alloys. The disadvantage of this system is that the transuranic target produces long-lived radionuclides in addition to those being transmuted.

The most detailed and comprehensive research conducted for accelerator-based waste transmutation began in 1992 by Los Alamos National Laboratory [11]. This included analysis of structural activation of accelerator components, target/blanket designs, liquid metal corrosion issues, and radiation damage of target and structural components [12-16]. The majority of these studies were computational in nature.

Several studies have occurred outside the U.S. as well. Detailed work was performed as part of the Japanese Omega program which was started in 1988 [17]. Studies of ADS at KTH started in 1993 [18]. Shortly after this, the CERN proposal of thorium-fueled ADS attracted a lot of attention in international media [19]. While various concepts have been suggested, the attention of the detailed design work in Japan,

Korea, the United States and Europe is now firmly focused on fast neutron spectrum, solid fuelled cores being supplied with source neutrons from a spallation neutron source.

I.C.2. Muse Experiments

Since 1997, the hybrid reactor group from Grenoble has been involved in an experimental program called MUSE (MUltiplication de Source Externe) in collaboration with the French CEA (Commissariat à l'Énergie Atomique), EDF (Electricité de France), and FRAMATOME. This experimental program takes place at the research reactor MASURCA (MAquette de SURgénérateur à CAdarache) of the CEA Nuclear Center of Cadarache. It is devoted to the study of neutronics in a fast sub-critical core subjected to an external neutron source. MUSE also studies the validation of correlated calculation codes. The measurements done during these experiments served as a test for the characterization of the neutron flux in a sub-critical medium, driven by an external source [20].

Dynamic experiments were carried out by operating the reactor in a sub-critical mode with a k_{eff}=0.86 and with a D-T neutron source (yield of 3×10^4 neutrons/pulse). The preliminary results were encouraging. The results have shown that there is a non-global response of the sub-critical block to a neutron pulse, the response depends both on local flux and energy spectrum. This data is very valuable for understanding the kinetics of the sub-critical media.

I.C.3. TRADE Experiments

TRADE (TRiga Accelerator Driven Experiments) was the result of collective effort of a working group composed by ENEA, CEA, CERN ANSALDO under Carlo Rubbia (ENEA) and Massimo Salvatores (CEA). The TRADE experiment was to be performed in the TRIGA reactor of the ENEA Cassaccia Center and consists of the coupling of an external proton accelerator to a target to be installed in the central thimble of the reactor with the reactor placed in a subcritical configuration. The pilot experiment was aimed at global demonstration of the ADS concept [21]. The TRADE experiments however have been recently abandoned by the ENEA due to high costs.

I.D. Project Overview

The next section of this thesis will describe the accelerator driven neutron source target design and analysis. Following that section, analysis of the use of that source in the UT NETL reactor will be given with special emphasis on the heat generation rates capable in the system with an electron LINAC source. Section IV details the design of a spent fuel experiment at TAMU using the neutron source design from Section II and again with special emphasis on heat generation rates.

II. ACCELERATOR DRIVEN NEUTRON SOURCE DESIGN

An accelerator driven neutron source for use in the RACE experiments was designed. Coupled electron-photon-neutron simulations were performed using MCNP-5 [22]. The target optimization was performed to optimize the neutron leakage from the target.

There are several parameters which influence the neutron production and leakage of the neutrons produced. These include:

1. Type of incident particle,
2. Energy of incident particle,
3. Location and size of beam on target,
4. Target geometry (cylindrical, hexagonal, conical, etc.),
5. Target material, and
6. Target dimensions.

In all cases, it was assumed that the electron LINAC produced electrons of 40 MeV in energy and with a beam spot of 1.0 cm in diameter. It was also assumed that all targets would be cylindrical in geometry due to simplicity of design and construction. Since it was assumed that the first four of these parameters were fixed, target optimization was performed by varying the target materials and dimensions. Three source materials were considered: lead, tungsten, and a tungsten-copper alloy. These target materials were then optimized for target radius and length using bare target calculations. MCNP input decks for the optimized targets can be found in Appendix A.

II.A. Lead Target Optimization

The length and radius of this target was varied to determine the optimal target dimensions. The radius was varied from a radius of ~1.5 cm to a radius of ~10.0 cm. The outgoing neutron current from the source versus target radius as calculated by MCNP-5 is shown in Fig. 1. As can be seen from Fig. 1, an optimal target radius exists at ~5.5 cm. The target length was then varied from ~5 cm to ~40 cm and the results are shown in Fig. 2. These simulations showed that there was no significant increase in exiting neutron current at target lengths greater than 10 cm. The optimal target dimensions were calculated to be 5.4 cm in radius and 25.0 cm in length. These dimensions are also sufficiently small to allow the target to easily fit into the space available in the reactors.

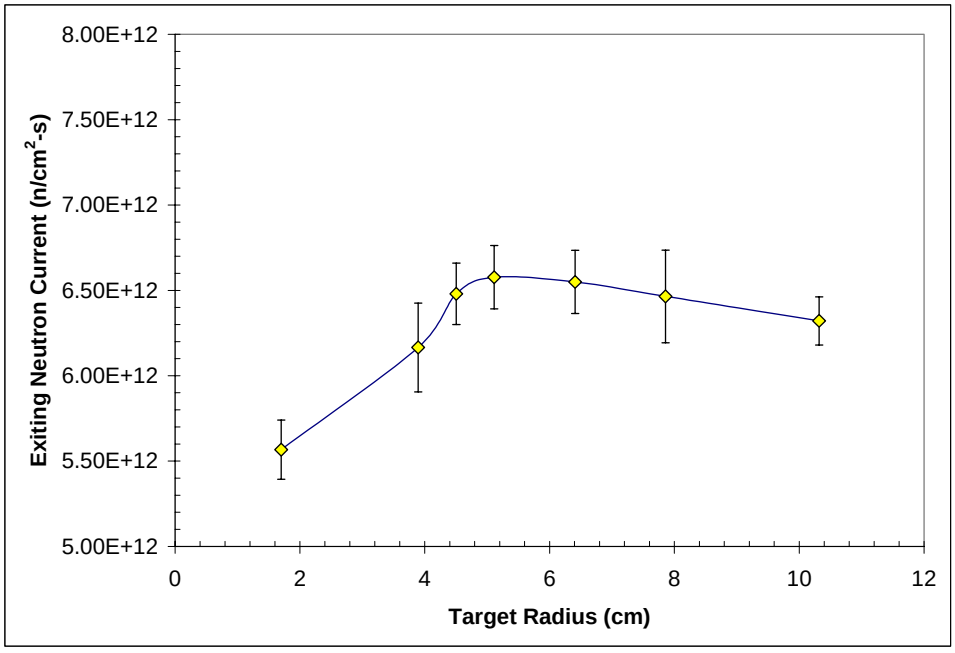

Fig. 1. Exiting neutron current versus target radius for lead target.

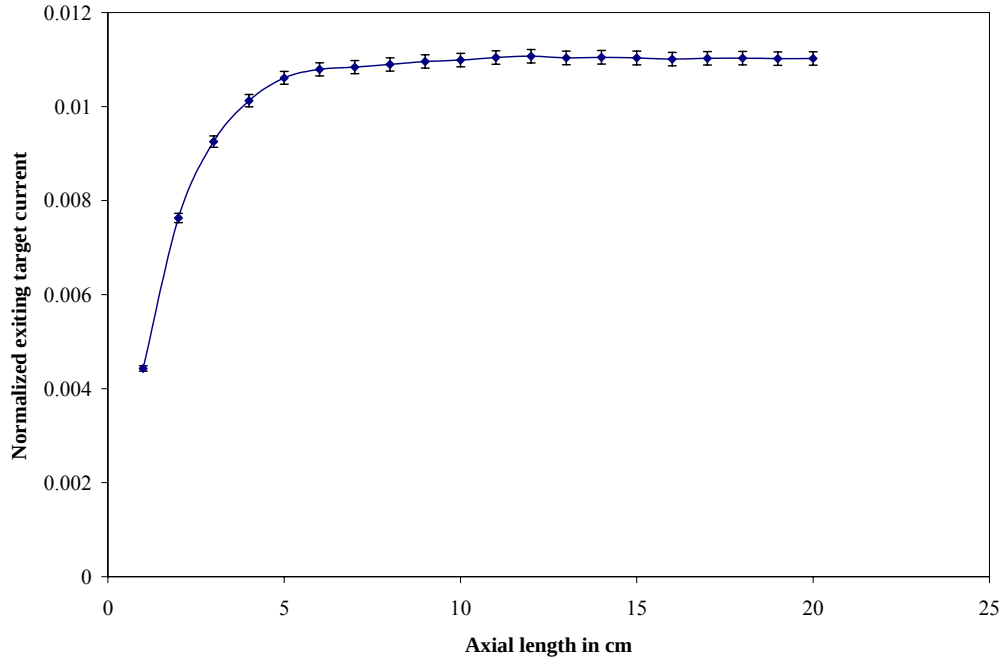

Fig. 2. Exiting neutron current versus target length for lead target.

It should be noted that the choice of lead as a target material is only for the purpose of this feasibility and scoping study. Since lead has such a low melting point, it is advantageous in RACE to use a tungsten (or tungsten alloy) target instead of a lead target. Past studies have focused heavily on lead and lead-bismuth targets. Thus, lead was included here to allow for easier comparisons to other works.

II.A.1. MCNP Parameter Optimization

In the process of the target dimension optimization, the *phys* cards in MCNP were also optimized. These cards are integral deciding factors for the computational time

and solution mechanisms used by MCNP for they determine the detail with which MCNP treats photon and electron interaction physics. These cards were optimized to provide the most detailed physics possible and to minimize computational time without effecting the neutron production.

The *phys* card optimizations were performed by iterating on the parameters used on each card. The following is the optimized *phys* cards for photons and electrons:

```
phys:p 1000 0 0 1 0
phys:e 50   0 0 0 0 10 1 0 1 0
```

The upper limit for electrons has been set as 50 MeV. This number is sufficient for these simulations since the incident electron beam is only 40 MeV. It was figured out that knock on electrons do not have any contribution in production of source neutrons and energy reduction of electron after collision has to be considered in continuous spectrum rather than predicting its probability. Higher production of neutrons per electron is obtained if electron-photon simulation is carried out with full bremsstrahlung angular distribution. However this switches off the photons striking the detector. This is the desired effect if we set fast detectors with gamma compensation. Doppler broadening and secondary electron contribution are significant. The reader is referred to the MCNP-5 manual for more information about these cards [22]. The *phys:p* card results in the following characteristics for the simulation:

1. upper limit for photons 1000 MeV
2. photons do produce electrons

3. coherent scattering occurs
4. biased photonuclear collision sampling
5. Doppler energy broadening occurs

The *phys:e* card results in the following characteristics for the simulation:

1. upper limit for electrons 50 MeV
2. photons will not produce electrons
3. electrons will produce photons
4. full bremsstrahlung tabular angular distribution
5. sampled straggling for electron energy loss
6. 10 times of bremsstrahlung photons production
7. x-ray photons produced by electrons
8. knock-on electrons will not be produced
9. photon induced secondary electrons produced
10. nominal bremsstrahlung production

II.B. Tungsten Target Optimization

Similar to the lead source optimization, the radius and length of the tungsten target was varied and the exiting current from MCNP-5 was recorded. Tungsten produced more neutrons for a smaller radius than that of the lead target. The p*hys* cards used were same as those used for the lead target. Plots of the exiting current versus radius and versus length are shown in Figs. 3 and 4, respectively. The optimized radius was found to be 3.0 cm with the length remaining at 25 cm.

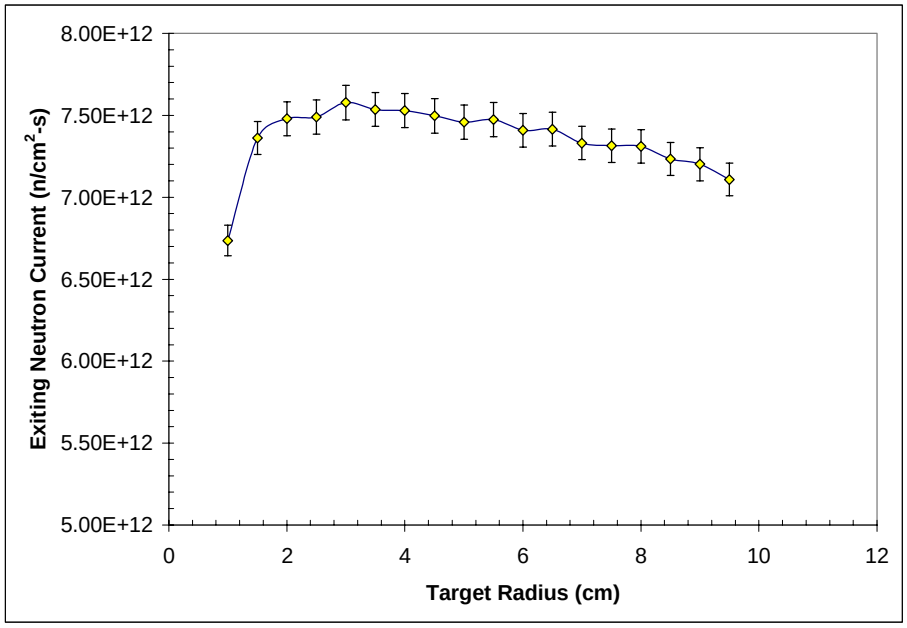

Fig. 3. Exiting neutron current versus target radius for tungsten target.

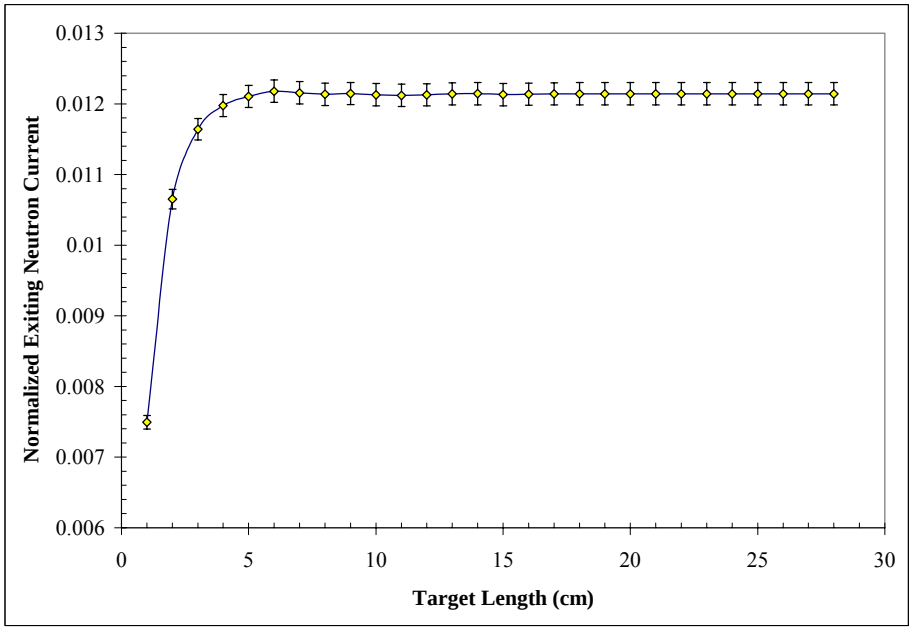

Fig. 4. Exiting neutron current versus target length for tungsten target.

It was interesting to note that as the radius was increased beyond the optimum value, the neutron production did not decrease by a substantial amount. This yielded the flexibility of using a bigger radius target, if desired, without resulting in a loss of neutron production. Also, we should note that the tungsten target produced nearly 15% more neutrons for the optimized radius when compared to the lead target.

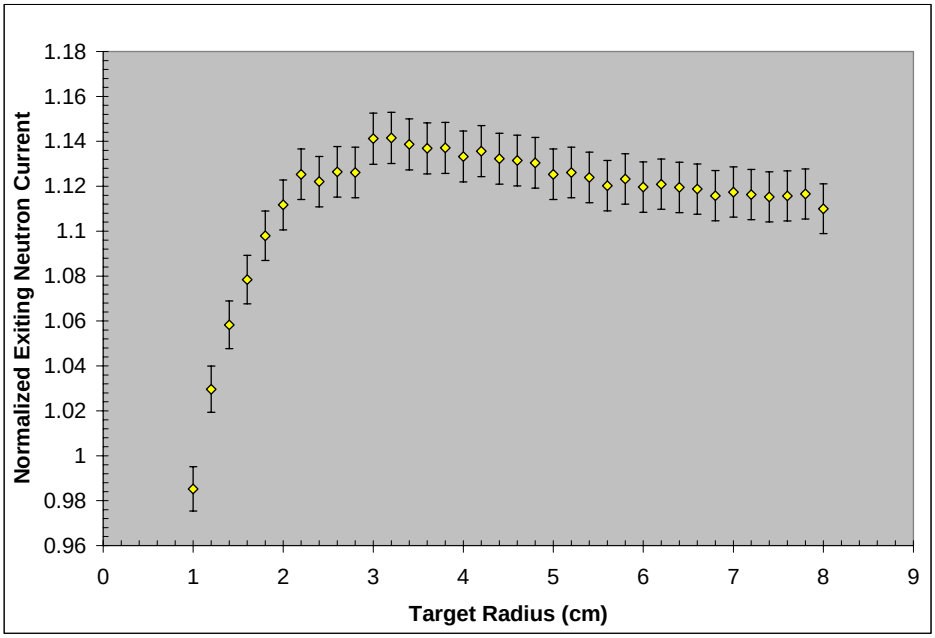

Fig. 5. Exiting neutron current versus target radius for W-Cu target.

II.C. Tungsten-Copper Alloy Target Optimization

The third kind of material considered was an alloy of tungsten. It consisted of 70% by weight tungsten and 30% by weight copper. The optimization was again performed by varying the radius and length of the target and recording the exiting neutron current (Figs. 5 and 6). The optimized radius was found to be 3.2 cm and 25 cm in length. It was noted that the inclusion of the copper has little effect on the neutron production; however, it makes the tungsten much easier to machine and braze.

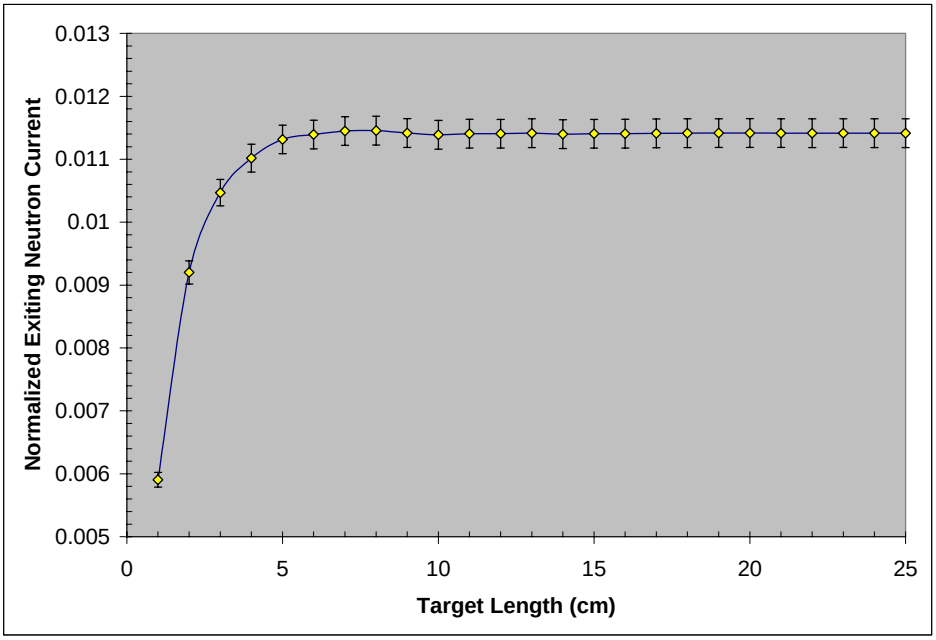

Fig. 6. Exiting neutron current versus target length for W-Cu target.

II.D. Target Cooling

There are two locations were the target can be inserted into the reactor. One location is in a beam port the other is inside the central area of the core. If the target is in the beam port, then there will be little to no cooling available from the air space in the beam port. In the beam port, there is no coolant for cooling the target. Thus, a cooling jacket was designed that would flow chill water around the target at a rate of 1.9 liters/min. This rate is sufficient for removing the heat generated in the target (up to 20 kW) using facility chill water at UT. The target with the cooling jacket is shown in Fig. 7.

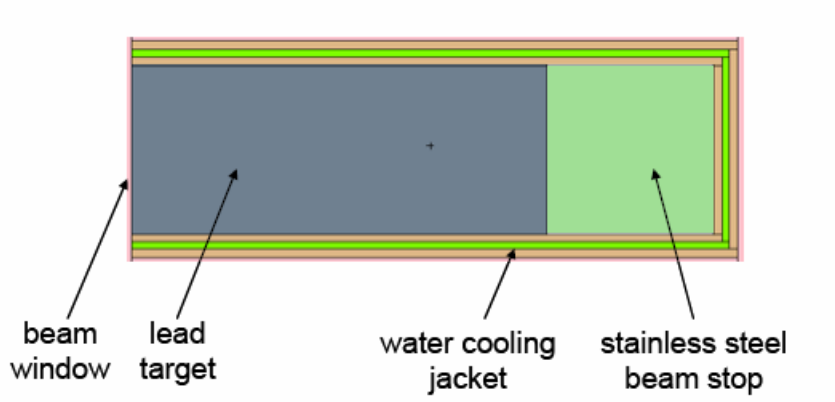

Fig. 7. Target with cooling jacket.

In case of the target being set inside the core, the cooling jacket is not required, since the pool water will provide cooling. This also implies that more heat can be added freely to the target (up to the limitations of the core cooling system).

III. ANALYSIS OF EXPERIMENTS USING UT NETL TRIGA REACTOR

III.A. Description of UT NETL

The UT Nuclear Engineering Teaching Laboratory (UT-NETL) houses a 1-MW TRIGA MARK–II nuclear research reactor. This reactor can be operated in two modes: pulse and steady-state. Safety analysis demonstrates that safe operation at power levels as high as 1.5-MW steady-state and 8400-MW peak pulse power is feasible. Pulse mode operation takes place by step reactivity insertions with reactor power initially at a power level of less than 1 kW. The maximum step reactivity insertion of 2.2% δk/k ($3.14) will produce a peak reactor power of approximately 1700 MW with a prompt energy release of 21 MW-sec. The safety of the TRIGA fuel arises from a large, prompt negative temperature coefficient that is characteristic of U-ZrH fuel moderator elements used in TRIGA systems. As the fuel temperature increases, temperature coefficient immediately compensates for reactivity insertions. The result is that reactor power excursions are terminated quickly and safely. The primary design characteristics for the UT-NETL reactor are given in Table I. A schematic of the core layout is shown in Fig. 8.

TABLE I

Principal Design Characteristics of the UT-NETL Reactor

REACTOR TYPE	TRIGA MARK – II
STEADY-STATE POWER (MAXIMUM)	1.1 MW (1.5 MW DESIGN)
PULSE POWER (MAXIMUM)	2.2 % δk/k ($3.14)
FUEL ELEMENT DESIGN	
FUEL – MODERATOR MATERIAL	U-ZrH
H/Zr RATIO	1.6 (1.65 MAXIMUM)
URANIUM CONTENT	8.5 WT %
URANIUM ENRICHMENT	19.7% U -235
SHAPE	CYLINDRICAL
LENGTH OF FUEL	38 CM
DIAMETER OF FUEL	3.63 CM
CLADDING MATERIAL	304 STAINLESS STEEL
CLADDING THICKNESS	0.051 CM
NUMBER OF FUEL ELEMENTS	
CRITICAL CORE	~ 64
OPERATIONAL CORE	~ 90
EXCESS REACTIVITY (MAXIMUM)	4.9 % δk/k
NUMBER OF CONTROL RODS	4
TRANSIENT (W / AIR FOLLOWER)	1
REGULATIN (W / FUEL FOLLOWER)	1
SHIM (W / FUEL FOLLOWER)	2
TOTAL REACTIVITY WORTH OF RODS	8.7 % δk/k
REACTOR COOLING	NATURAL CONVECTION OF POOL WATER

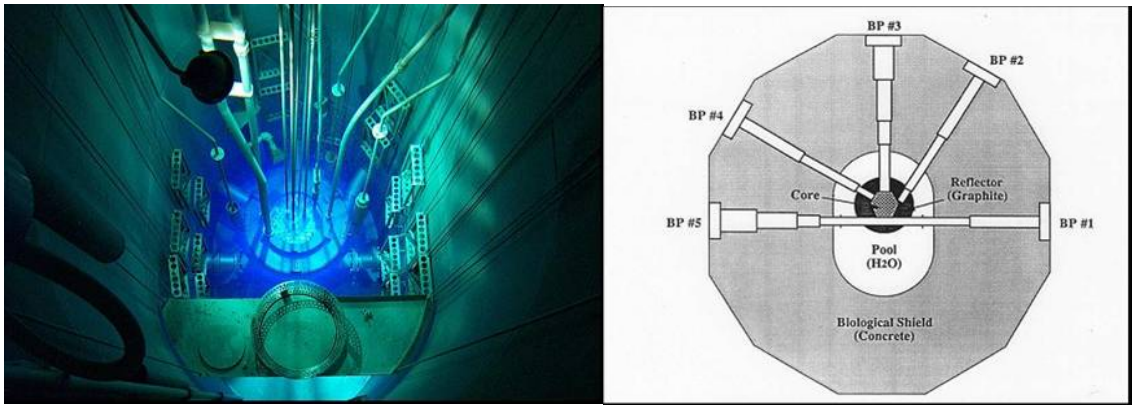

Fig. 8. UT-NETL TRIGA reactor under operation and cross sectional core layout.

III.B. Analysis of Experimental Arrangements at UT NETL

The target designed in Section II will be inserted into the UT NETL core, coupled with a 40 MeV electron LINAC (operating at 4-kW of beam power), and used to drive the core in a subcritical configuration. Two core locations were proposed for the target: one in beam port #5 (a tangential through tube port, Fig. 8) and the other in the core central thimble. Irradiation in the beam port would allow for a relatively simple test (i.e., requiring no fuel movement) at low power. The target in the central thimble will allow for the highest possible heat generation and is most relevant to proposed ADS operation. Four experimental cases were analyzed to determine the feasibility of these experiments. These cases are as follows:

1. Target located in beam port #5 (BP#5).
2. Target located in core central thimble.

3. Target located in core central thimble and control rods moved out one ring.
4. Target located in core central thimble and control rods moved out two rings.

A full core MCNP model for the UT NETL reactor was constructed. This model explicitly simulated all fuel rods, control rods, graphite rods, graphite reflector, beam ports, and pool water. The physical domain of the model ended at the pool wall. Each case was simulated in MCNP and the heat generation rate in the fuel was recorded. For the purposes of observing thermal feedback effects, heat generation rates above 1 kW were desired. Simulations were performed for all three optimized target materials (i.e., lead, tungsten, and tungsten-copper). The results for each case are reported in the following sections.

III.B.1. Core Arrangement #1

In this arrangement, the target was placed in BP#5 as close to the fuel as possible. The target had a cooling jacket in place for heat removal. The target had a radius of 5.0 cm. The cladding on the target was 0.5 cm thick, the cooling gap was 0.4 cm thick, and the outer jacket was 0.5 cm thick. The electron beam entered the target from the BP#5 side. A thin beryllium window (0.001 cm thick) faced the electron beam (as per the optimized target shown in Fig. 7). A schematic of the target in position in BP#5 is shown in Fig. 9. The MCNP-5 calculated heat generation rate in the fuel for this arrangement using the lead target is shown in Table II. Varying levels of subcriticality were simulated by modifying the control rod heights in MCNP until a k_{eff} of 0.95, 0.98, and 0.99 were achieved.

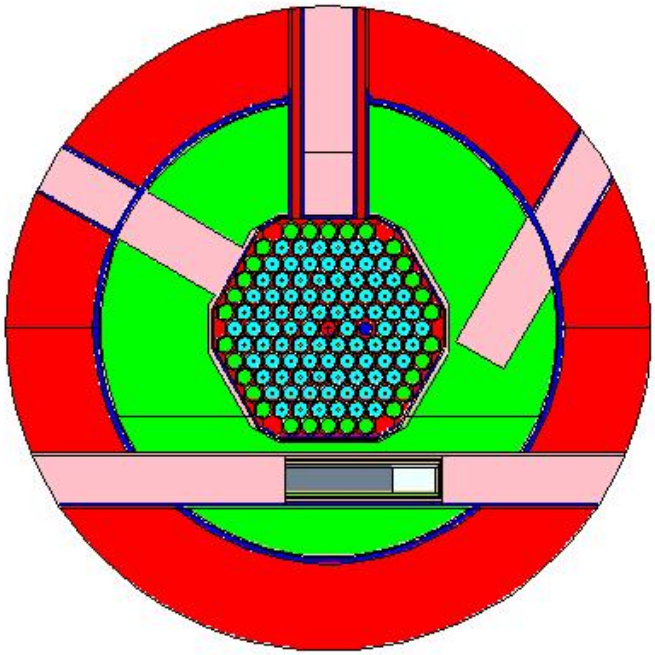

Fig. 9. Screen capture of MCNP geometry for UT–NETL experiment with accelerator source in beam port # 5.

TABLE II

Heat Generation Rate for Lead Target in BP#5

k_{eff}	**Heat Generation Rate (kW)**
0.9502 +/- 0.0007	0.58 +/- 0.055
0.9800 +/- 0.0004	0.735 +/- 0.075
0.9901 +/- 0.0004	1.22 +/- 0.145

For safety purposes, k_{eff} will not be allowed to exceed 0.99. At that level of subcriticality, the heat generation rate is approximately 1.2 kW. The primary reason for this low value is that only 1/3rd of the neutrons emitted from target are entering the fuel region. Many neutrons are leaking from the core. This is because the neutrons in the target are emitted isotropically and since only 120 degrees of the target is facing the fuel. Though 1.2 kW is within the range of interest for these experiments, it leaves little chance for error and little opportunity to operate the system at lower k_{eff} values.

The lead target was then replaced with tungsten and tungsten-copper and the simulations repeated. The calculated heat generation rates for the tungsten and tungsten-copper targets in BP#5 are shown in Tables III and IV, respectively. The heat generation rates obtained at k_{eff}=0.99 for both targets are sufficient for obtaining the desired negative fuel temperature feedback; however, again the system cannot be operated at lower k_{eff} values. It was noted that the tungsten targets were sufficiently superior to the lead target but that the two tungsten targets were not statistically different in heat generation rates.

TABLE III

Heat Generation Rate for Tungsten Target in BP#5

k_{eff}	**Heat Generation Rate (kW)**
0.9509 +/- 0.0007	0.46 +/- 0.02
0.9804 +/- 0.0007	1.06 +/- 0.08
0.9903 +/- 0.0007	2.07 +/- 0.165

TABLE IV

Heat Generation Rate for Tungsten-Copper Target in BP#5

k_{eff}	**Heat Generation Rate (kW)**
0.9510 +/- 0.0006	0.56 +/- 0.02
0.9810 +/- 0.0006	1.21 +/- 0.08
0.9896 +/- 0.0007	2.15 +/- 0.15

III.B.2. Core Arrangement #2

In this arrangement, the target was placed in the central thimble in the UT-NETL core. The cooling jacket was removed and pool water was used to cool the source. The target had a radius of 3.506 cm and was 25.0 cm long. The stainless steel cladding on the target was 0.574 cm thick. The electron beam entered the target from above. A thin beryllium window (0.001 cm thick) faced the electron beam for the lead target but was removed for the tungsten targets. A stainless steel beam stop of 4 cm in thickness was attached to the end of the target. The top of the target was in parallel with the top of the fuel meat for the fuel elements. A schematic of the target in position is shown in Fig. 10. The MCNP-5 calculated heat generation rates in the fuel for this arrangement and the lead, tungsten, and tungsten-copper targets are shown in Tables V, VI, and VII. As can be seen the results from all of these simulations are the same or lower than those from core arrangement #1. This is due to the high absorption of neutrons by the water between the target and the fuel and by the absorption of neutrons in the control rods.

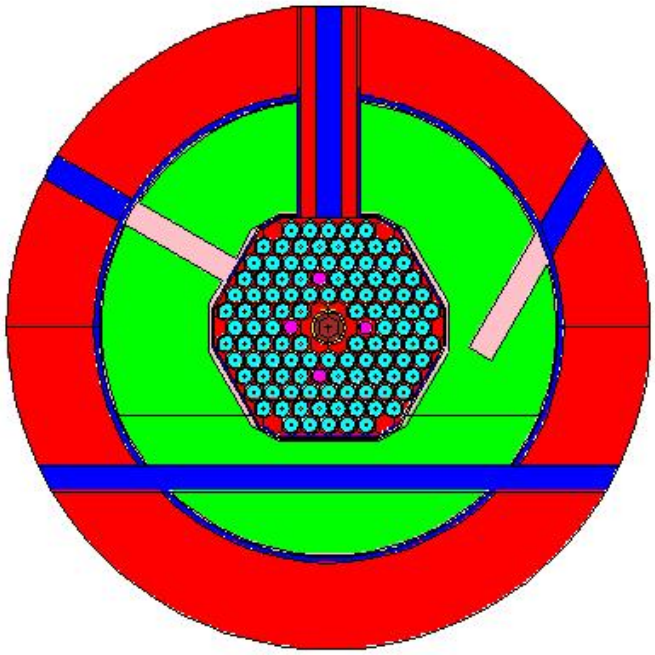

Fig. 10. Screen capture of MCNP geometry for UT–NETL experiment with accelerator source target at the center of the core.

TABLE V

Heat Generation Rate for Lead Target in Core Arrangement #2

k_{eff}	**Heat Generation Rate (kW)**
0.9500 +/- 0.0007	0.065 +/- 0.02
0.9800 +/- 0.0007	0.13 +/- 0.01
0.9900 +/- 0.0007	0.315 +/- 0.04

TABLE VI

Heat Generation Rate for Tungsten Target in Core Arrangement #2

k_{eff}	**Heat Generation Rate (kW)**
0.9468 +/- 0.0008	0.585 +/- 0.025
0.9801 +/- 0.0008	0.97 +/- 0.06
0.9901 +/- 0.0007	1.35 +/- 0.08

TABLE VII

Heat Generation Rate for Tungsten-Copper Target in Core Arrangement #2

k_{eff}	**Heat Generation Rate (kW)**
0.9468 +/- 0.0008	0.60 +/- 0.03
0.9801 +/- 0.0008	1.12 +/- 0.065
0.9901 +/- 0.0007	1.88 +/- 0.17

III.B.3. Core Arrangement #3

The target radius was re-optimized by varying its radius while inside the core and noting the heat generation rate. It was found that a larger target radius produced significantly more heat in the fuel. This is due primarily to the displacement of water between the target and the fuel. An optimized target radius of 4.206 cm was found with a stainless steel cladding thickness of 0.574 cm. Also to decrease absorption of source

neutrons in the control rods, the control rods were moved one ring out away from the target. Core arrangement #3 is shown in Fig. 11. The MCNP-5 calculated heat generation rates in the fuel for this arrangement and the lead, tungsten, and tungsten-copper targets are shown in Tables VIII, IX, and X.

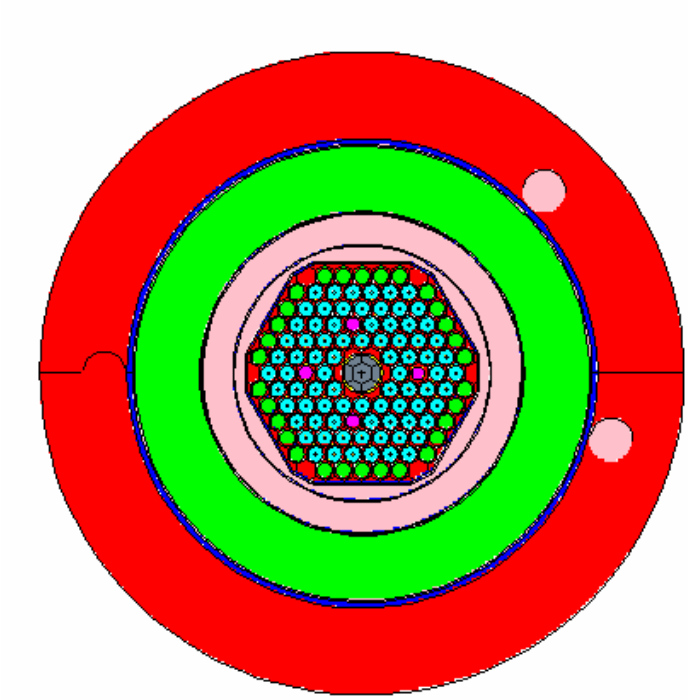

Fig. 11. Screen capture of MCNP geometry for UT–NETL experiment with target at the center of the core and control rods one fuel element away.

TABLE VIII

Heat Generation Rate for Lead Target in Core Arrangement #3

k_{eff}	**Heat Generation Rate (kW)**
0.9494 +/- 0.0008	0.845 +/- 0.035
0.9800 +/- 0.0008	1.735 +/- 0.115
0.9908 +/- 0.0007	2.47 +/- 0.165

TABLE IX

Heat Generation Rate for Tungsten Target in Core Arrangement #3

k_{eff}	**Heat Generation Rate (kW)**
0.9501 +/- 0.0007	0.63 +/- 0.03
0.9800 +/- 0.0007	1.21 +/- 0.075
0.9903 +/- 0.0006	2.045 +/- 0.15

TABLE X

Heat Generation Rate for Tungsten-Copper Target in Core Arrangement #3

k_{eff}	**Heat Generation Rate (kW)**
0.9501 +/- 0.0007	1.32 +/- 0.035
0.9805 +/- 0.0007	1.55 +/- 0.115
0.9901 +/- 0.0007	2.37 +/- 0.18

The heat generation rates (especially for the tungsten-copper target) has increased to almost 2.4 kW at k_{eff} =0.99. Thus moving the control rods away from the target and increasing the target size resulted in significantly higher heat generation. It should still be noted that the heat generation rate at lower k_{eff} values is still too small to allow for a realistic temperature feedback effect.

III.B.4. Core Arrangement #4

In order to determine if additional movement of the control rods away from the target would increase the system heat generation rates, an additional core arrangement was considered with the control rods moved out another ring from the center. In this case, these analyses were performed only for the tungsten-copper target. The target had a radius of 4.206 cm and a clad thickness 0.574 cm. The target is located such that the top of the target is in parallel with the top of the fuel meat. A schematic of this core arrangement is shown in Fig. 12.

Two additional perturbations to this arrangement were simulated. The target was then moved to two different axial positions: one such that the target top is 4 cm below the top of the fuel meat and the other such that the target top is 8 cm below the top of the fuel meat. All these simulations were performed with a k_{eff} =0.9900. The results for these simulations with different target axial locations are shown in Table XI. As can be seen, the heat generation rates from these simulations suggest that this experiment should be able to reach well within the temperature feedback regime.

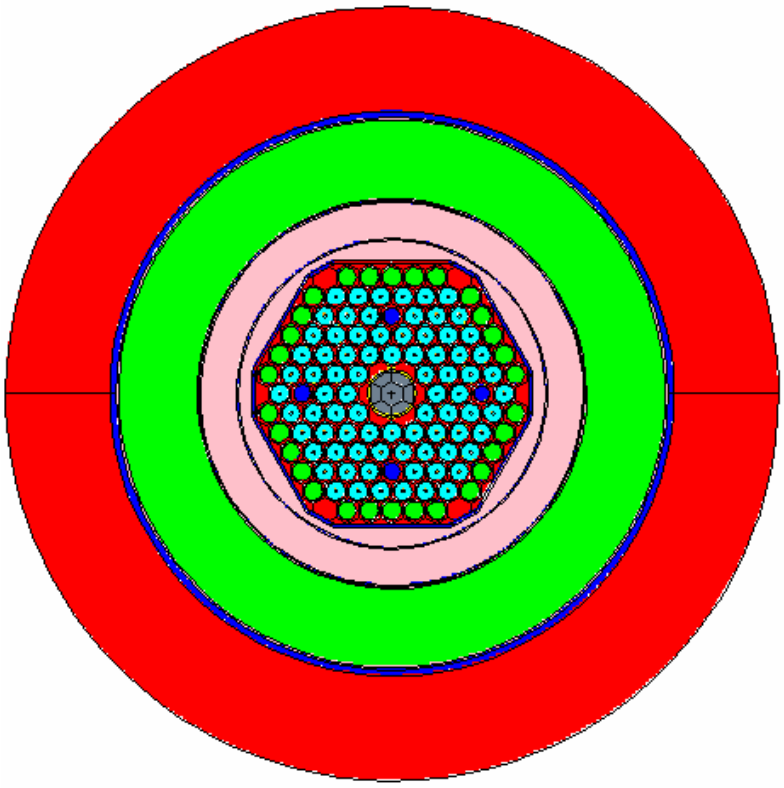

Fig. 12. Screen capture of MCNP geometry for UT–NETL experiment with target along with jacket at the center of the core and rods two fuel element away.

TABLE XI

Heat Generation Rate for Tungsten-Copper Target in Core Arrangement #4 with the Target Located at Different Axial Heights

Target Axial Location	**Heat Generation Rate (kW)**
in parallel with fuel meat	3.05 +/- 0.295
4 cm below fuel meat	3.475 +/- 0.21
8 cm below fuel meat	5.055 +/- 0.35

A set of simulations were also performed to analyze the effect of removing the cladding from the target. Again the tungsten-copper target was considered. One simulation considered simply removing the cladding. The other simulation considered removing the cladding and increasing the radius of the target. Schematics showing the target arrangement for these three simulations can be found in Fig. 13. In all cases the target was placed at 8 cm below the top of the fuel meat. The heat generation results for these three arrangements can be found in Table XII. As can be seen the target produces more heat with the cladding in place. This is due to the higher neutron absorption in the tungsten than in the stainless steel. Thus, it is preferred to retain the stainless steel cladding as a means for displacing water in the core.

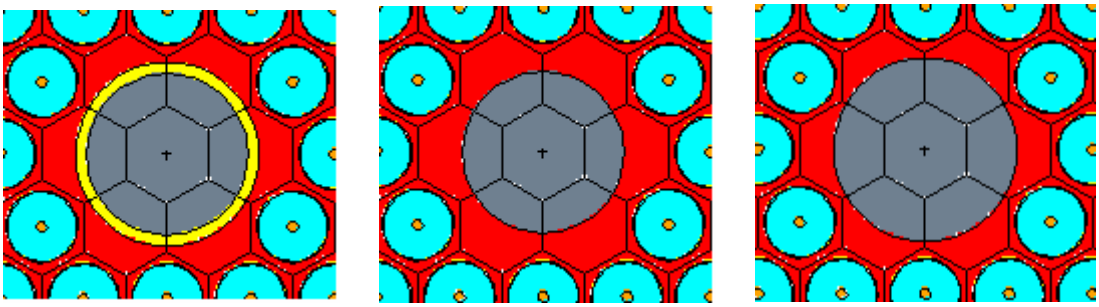

(a) (b) (c)

Fig. 13. Screen capture of MCNP geometry for UT–NETL experiment with accelerator source target at core center with (a) cladding, (b) no cladding, and (c) no cladding and larger radius.

TABLE XII

Heat Generation Rate for Tungsten-Copper Target in Core Arrangement #4 with the Target Located at Different Axial Heights

Target Axial Location	Heat Generation Rate (kW)
cladding	5.055 +/- 0.35
no cladding	4.44 +/- 0.20
no cladding and larger radius	4.45 +/- 0.225

III.C. Optimal Core Configuration for UT-NETL RACE

The optimized core configuration for the RACE experiments at the UT-NETL was determined based on the results from Section III.B. The optimal configuration consisted of the following:

1. Tungsten-copper target with a radius of 4.206 cm surrounded by a stainless steel cladding with a thickness of 0.574 cm.
2. The target located in the central thimble and 8 cm below the top of the fuel meat.
3. A 4-cm thick stainless steel beam stop included at the bottom of the target.
4. The control rods moved out two rings from the standard operating position.
5. The outer ring of the core occupied by graphite dummy elements.

An axial schematic of this core arrangement is shown in Fig. 14. A radial schematic of this core arrangement is shown in Fig. 12.

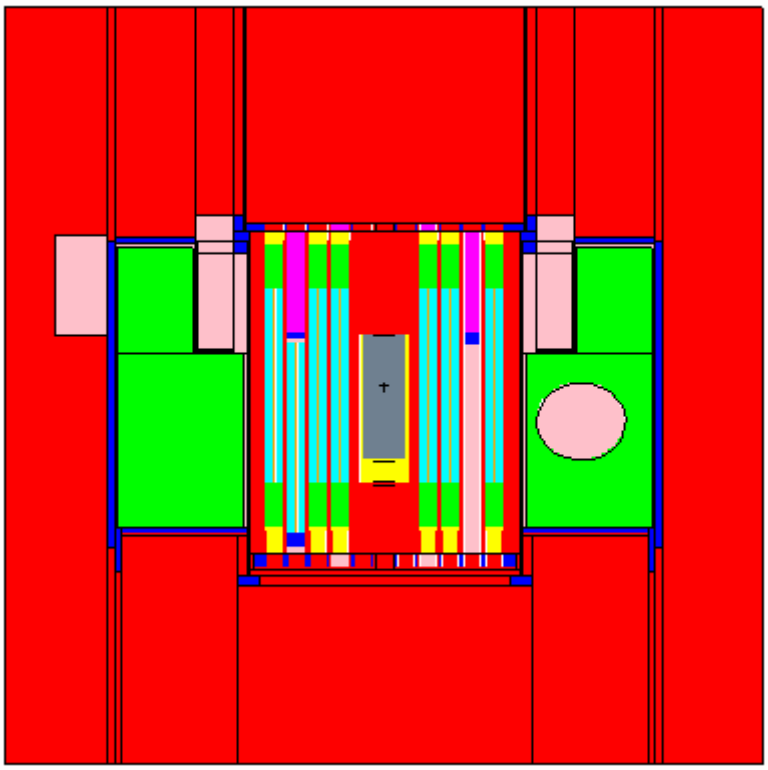

Fig. 14. Screen capture of axial view of the final design MCNP geometry for UT–NETL reactor accelerated coupled experiment.

Analysis of this optimized core arrangement was performed to allow for a better understanding of the expected experimental results. Plots of the k_{eff} versus rod position, heat generation rate versus rod position, and heat generation rate versus k_{eff} are shown in Figs. 15, 16, and 17, respectively.

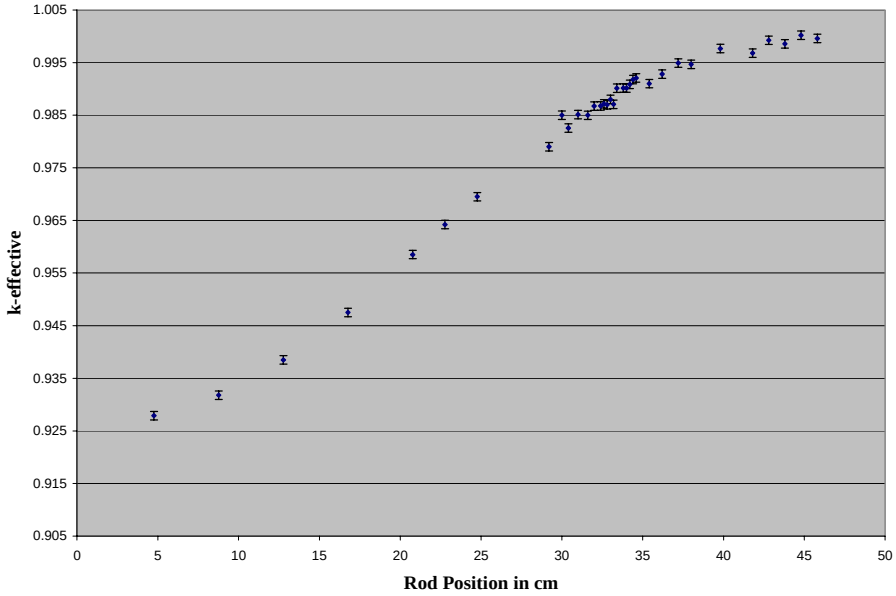

Fig. 15. k_{eff} versus control rod positions.

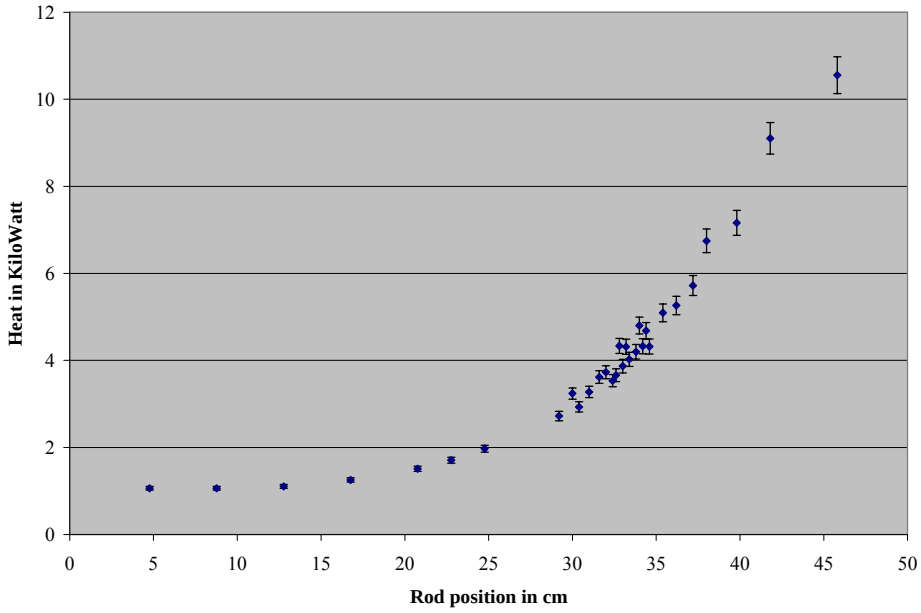

Fig. 16. Heat generation versus rod position.

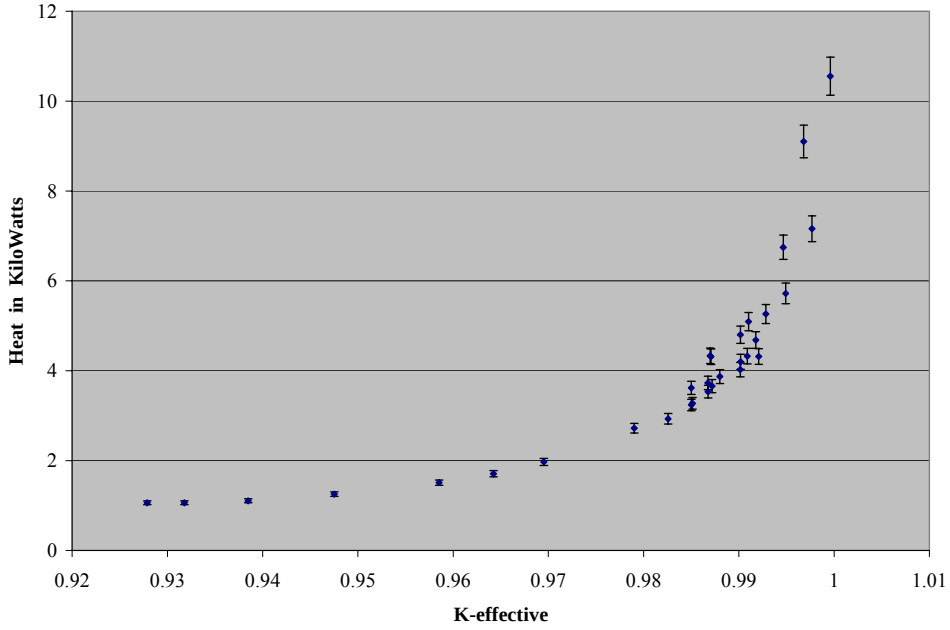

Fig. 17. Heat generation versus k_{eff}.

At the highest rod position, the bottom of the absorber is parallel to the top of the fuel meat. At the lowest rod position, the fuel follower is parallel to the bottom of the fuel element. As can be seen, k_{eff} can be varied from 0.975 to 0.999 and still produce over 3 kW of heat. This should provide flexibility to operate at wide range of subcriticality levels while still within the feedback regime. It should also be noted that with the target in place and rods fully withdrawn the system is still not critical though it is close. From these calculations, it has been shown that the RACE experiments using the UT-NETL core should provide a feasible mechanism for achieving an ADS experiment with temperature feedback over a wide range of subcriticality levels.

IV. TEXAS TRANSMUTATION SYSTEM DESIGN

One interest in the RACE program is in producing a permanent facility for studying ADS characteristics and to serve as an educational and training tool for ADS operation. A subcritical assembly composed of spent fuel discharged from the TAMU NSC TRIGA reactor will be designed and built for location in the NSC pool to serve this goal. The TRIGA reactor at TAMU has been in operation since 1961. Present at the facility is a complete core load of spent fuel. This spent fuel will be assembled into a subcritical lattice (within the existing NSC pool) with four internal accelerator driven target positions and three safety control rods. The system will be designed such that it will remain subcritical with the control rods completely removed from the core. Thus, the control rods only serve as shutdown safety rods, but can also be used to operate the system at lower levels of subcriticality as well. This experimental system will allow for evaluation of the ADS with the accelerator source in different locations in the core. The system will also serve as a teaching tool since its design maintains the system in a subcritical configuration and thus is more "student-friendly". This design has been named the Texas Transmutation System (TTS).

IV.A. History of TAMU NSC Reactor

The Nuclear Science Center Reactor (NSCR) operated from 1962 until 1967 with MTR-type curved aluminum plate elements. During this time the reactor was operated extensively at a maximum power level of 100 KW. In 1968, the reactor was converted to

General Atomic TRIGA type fuel rods and the maximum power level was increased to 1.0 MW. The initial core loading produced satisfactory operation, but the experimental facility was soon affected by both fuel burnup and samarium buildup. To restore excess reactivity, additional fuel was periodically added to the core and a graphite reflector was added to all four surfaces. This eventually led to 126 element core with a resultant decrease in flux of almost 40% and the elimination of most of the irradiation facilities.

In August, 1970, fuel followed rods were installed to help solve the problem of maintaining excess reactivity. This installation required modification of the grid plate to allow passage of the fueled portion of the control rod through the grid plate. An average reactivity increase of $ 1.10 per fueled follower was achieved which extended the core life by nearly two years. The high burnup rate of standard TRIGA cores continued to be an operational problem for the NSCR which operated at a burnup of approximately 100 MW-days per year since 1969.

General Atomic FLIP (Fuel Life Improvement Program) fuel was designed to replace standard TRIGA fuel elements. FLIP fuel has the same dimensions as standard TRIGA fuel and differs only in material composition. The enrichment was increased from 20% to 70%, the hydrogen to zirconium ratio was decreased from approximately 1.7 to 1.6, and 1.5 weight percent natural erbium was added as burnable poison. FLIP fuel has an expected lifetime of 9 MW-years which is considerably higher than the ½ MW-year lifetime of standard fuel.

Since funds were not available for a complete FLIP core, the initial core operated with a mixture of FLIP and standard TRIGA fuel. A precedent for this had been established by General Atomic when they operated a standard core loaded with eighteen centrally located FLIP elements in a fuel test program. Calculations were performed at Texas A&M which led to the conclusion that satisfactory core arrangements were possible with a mixed core. The NSCR operated with two mixed core loadings containing 35 FLIP elements and 59 FLIP elements each between 1973 and 1979. As funds became available, the amount of FLIP fuel was increased until a complete FLIP loading was achieved.

By 1979, all standard fuel had been replaced and cores V-VIII were operated with FLIP fuel only. From 1979 to the present, the maximum power level has remained at 1.0 MW.

IV.B. TTS Design Concept

TTS is a multi-target sub-critical assembly of standard TRIGA fuel driven by an electron accelerator. This system will make use of the complete core load of spent fuel available at the NSC. This spent fuel will be assembled into a subcritical lattice (within the existing NSC pool) with four internal accelerator driven target positions and three safety control rods (Fig. 18). The system will be designed such that it will remain subcritical with the control rods completely removed from the core. Thus, the control rods only serve as shutdown safety rods, but can also be used to operate the system at lower levels of subcriticality as well.

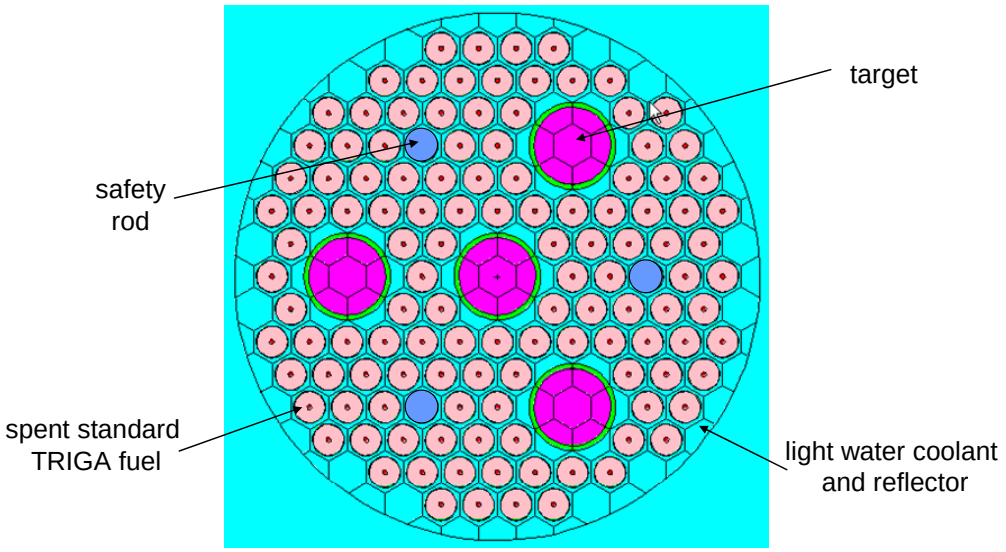

Fig. 18. MCNP geometry of TTS TAMU with four target positions

TABLE XIII

Heat Generation Rate for TTS Design

k_{eff}	**Heat Generation Rate (kW)**
0.942 +/- 0.001	5.37 +/- 0.18

MCNP simulations were performed to evaluate the initial TTS design. A copy of the TTS input deck can be found in Appendix C. The system was modeled explicitly and a 40-MeV, 100-μA electron beam was impacted on the center of all the targets in the design. The heat generation rate in the fuel was then tallied. There are in total 120 standard fuel elements in a close packing in the TTS. The fuel isotopics was calculated

using a two-dimensional HELIOS calculation for the NSC TRIGA reactor. The isotopics included in MCNP however only included the decrease in actinide content due to burnup and all fission products were included as one average fission product in MCNP. In future efforts for designing TTS, a more detailed fuel mixture will be used. The result for the calculated heat generation rate for TTS is shown in Table XIII. As can be seen, even with a low level of subcriticality, the TTS system produces sufficient heat to allow for operation in the temperature feedback regime for TRIGA reactor fuel.

IV.C. TTS Evaluation Results

In addition to the total heat generation rate shown in Table XIII, heat generation rates in individual elements in TTS were tallied to show the spatial distribution of heat production. Specifically, the interest was in determining that there were not any particular rods that were subjected to a heat load beyond the design basis for TRIGA fuel (which is approximately 35 kW per fuel element). Also, heat generation rates in the targets were tallied to determine the heat load on the targets. Again, the targets will be cooled by natural circulation in the NSC pool and the heat loads on the targets must remain below the fuel element design basis to ensure appropriate cooling. The heat generated in each of the elements is due to three sources: (1) non-fission neutron reactions (mainly elastic and inelastic scattering), (2) neutron-induced fission reactions, and (3) photon reactions. For tallying these results, *f7:n* and *f6:p* tallies in MCNP-5 were used. It should be noted that energy deposition due to electron slowing down was not tallied; however, it is assumed that almost all of the power from the accelerator beam (4

kW) will be deposited locally as heat in the target. The heat deposition in the targets for neutron reactions, photon reactions, and all neutron and photon reactions is shown in Figs 19, 20, and 21, respectively. As can be seen the heat deposition in the target is well below the single element limits for the system and this energy deposition is due almost entirely to photon energy deposition.

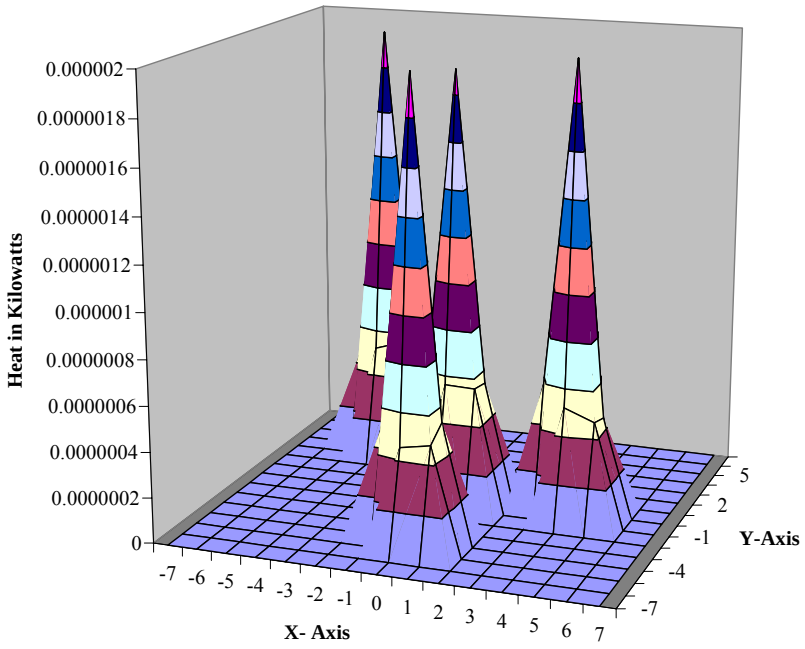

Fig. 19. Heat generation in the four targets due to neutron reactions.

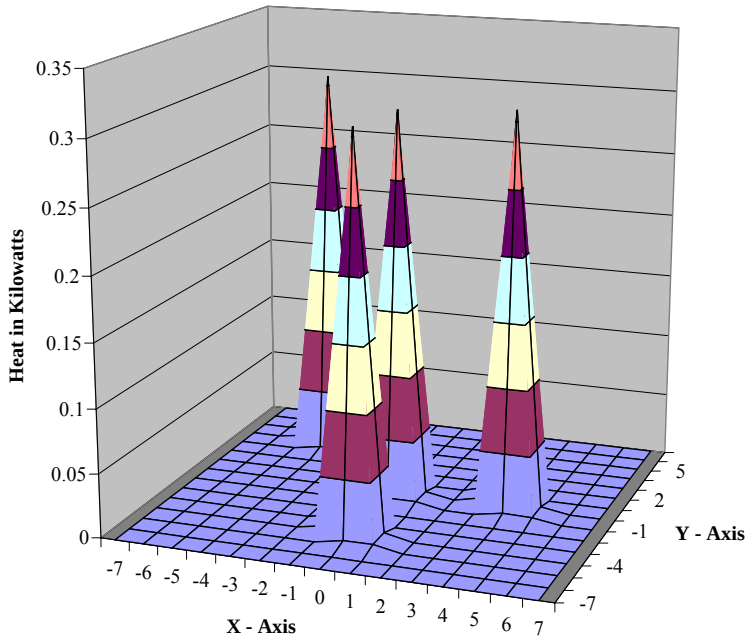

Fig. 20. Heat production in the four targets due to photon reactions.

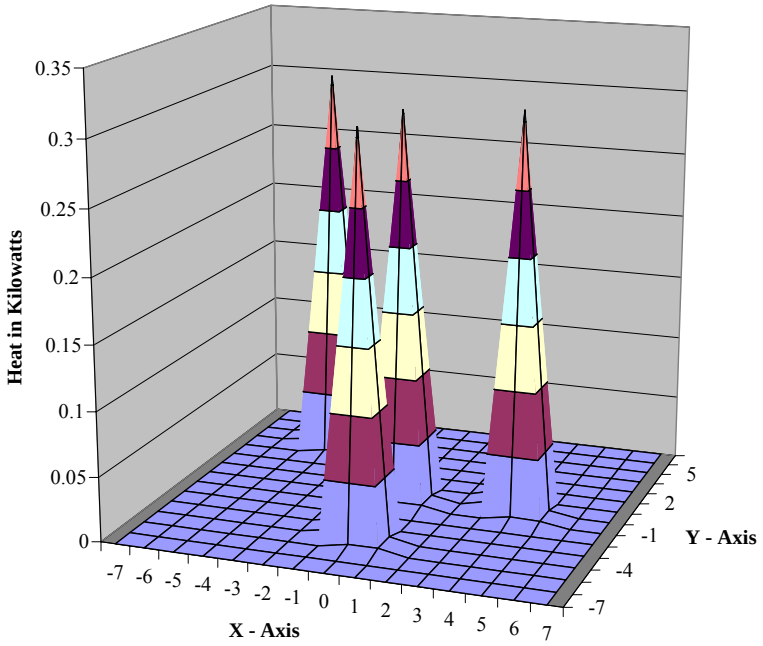

Fig. 21. Total heat production in the four targets.

The heat deposition in the fuel elements for neutron reactions, photon reactions, and all neutron and photon reactions total is shown in Figs 22, 23, and 24, respectively. Again it can be seen that the heat deposition in any single element is well below the limits for TRIGA reactor fuel. Thus, cooling concerns for this system should be insignificant.

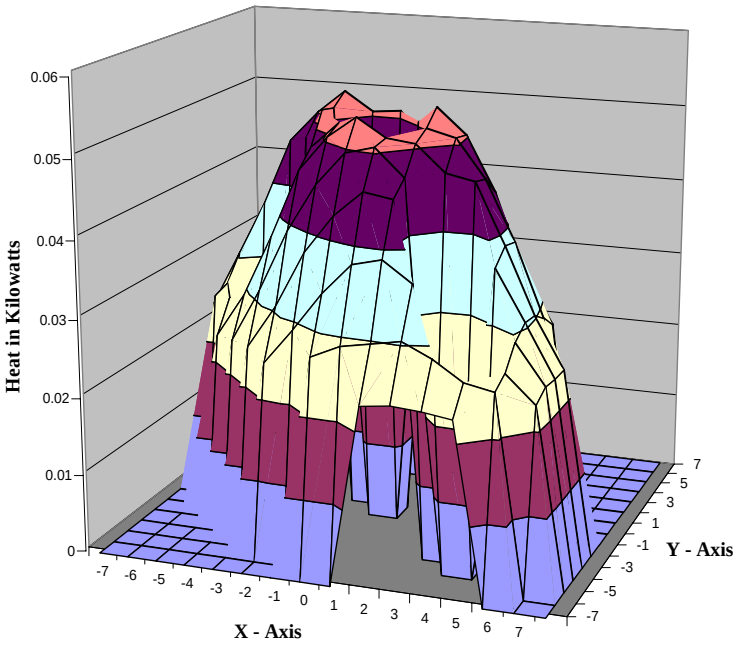

Fig. 22. Heat generation rate in fuel due to neutron reactions.

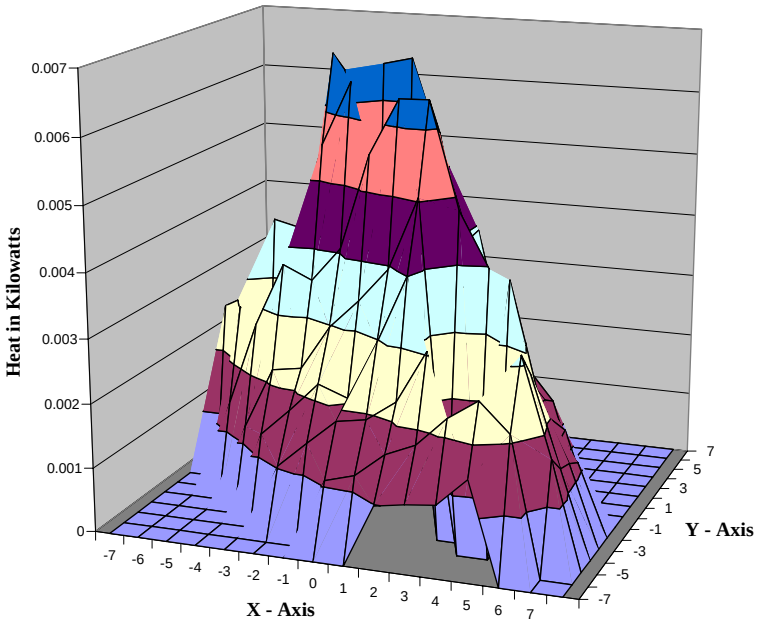

Fig. 23. Heat generation rate in the fuel due to photon reactions.

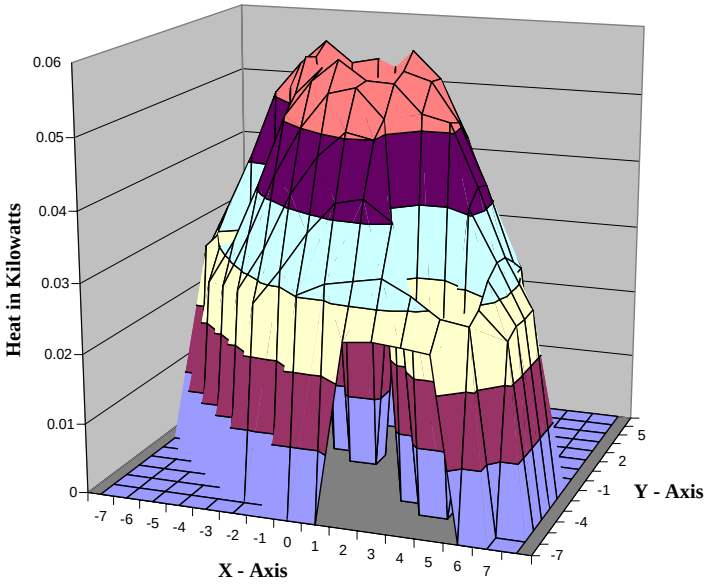

Fig. 24. Total heat generation rate in fuel.

It has been shown that the heating rates in the TTS are expected to provide sufficient temperature in the fuel to produce measurable temperature feedback effects. This will allow for transient and steady-state studies of ADS operation under feedback conditions. These experiments will be used to provide benchmark data for development of ADS code systems.

V. CONCLUSIONS

The objective of this feasibility study was to aid in the development of subcritical accelerator driven systems with feedback. The current operational and experimental experience with such systems is effectively non-existent. These experiments will provide the first dataset for such conditions.

Design of a tungsten-copper target for the production of neutrons from a 40 MeV, 100 μA electron accelerator was performed. The optimized target geometry was found to be that of a right circular cylinder with a radius of 3.2 cm and a length of 25 cm. This target will produce a neutron source of approximately 10^{12} neutrons per second. It should be noted that for this accelerator driven target, the neutron source strength is relatively insensitive to the radius and length of the target. This allows for more flexibility in altering the target dimensions to allow for incorporation in different ADS configurations.

For the purposes of observing temperature feedback in the RACE systems, heat generation rates for the total systems were needed to be above 1 kW and preferably above 5 kW. All simulations used a 40-MeV, 100-μA accelerator beam. It was shown that with this accelerator the configuration #4 for the UT-NETL reactor using a tungsten-copper target will provide 5.05 kW of heat generation with a k_{eff}=0.99 and 1.25 kW of heat generation with a k_{eff}=0.95. This will provide sufficient heat for temperature feedback operation over a wide range of subcriticality levels.

The overheating of the target may determine the limit for the maximum current of the accelerator and thus the total heat generation in the system. To compensate for this limitation, a multi-target system named the TTS was analyzed. It was shown that the TTS system would provide excellent heat production over a wide range of subcriticality levels and could serve as a permanent experimental system for teaching and training the next generation of nuclear scientists and engineers.

Operationally, the RACE program is intended to consist of a number of experiments which will be used a benchmarks for steady-state and transient operation of ADS. It has been shown that with modest accelerator capabilities, two experiments could be performed which would allow for operation in a temperature feedback regime. It is the recommendation of this thesis that the experiments begin with beam port experiments (core arrangement #1 from Section III) using a cooling jacket. This will provide for low power experiments that could be performed over a wide range of subcriticalities without any impact on normal reactor configuration or operation. Following these experiments, the target would be moved internal to the reactor (core configuration #4 from Section III) and experiments would be performed that would be well within the temperature feedback regime of the TRIGA fuel. Following this experiments could be performed with the TTS arrangement at TAMU and allow for a wider range of experiments over a longer time period (since this would not impact reactor operation in any way). Finally, it should be noted that if a higher current accelerator system could be acquired (for example a 25 kW accelerator similar to

industrial irradiator systems currently in use), then the heat generation rates in these system could well exceed 80-100 kW. These calculations have shown that the feasibility of the RACE program is well within the capabilities of existing systems and arrangements for performing the experiments should proceed accordingly.

REFERENCES

1. U.S. Department of Energy, "A Roadmap for Developing ATW Technology," Report to Congress (1999).
2. R.G. Cochran and N. Tsoulfanidis, *The Nuclear Fuel Cycle: Analysis and Management*, American Nuclear Society, La Grange Park, IL (1990).
3. W.C. Sailor, C.A. Beard, F. Venneri, and J.W. Davidson, "Comparison of Accelerator-Based with Reactor-Based Nuclear Waste Transmutation Schemes," *Prog. Nucl. Energy,* **28**(4), 359 (1994).
4. C.A. Beard, J.W. Davidson, R.A. Krakowski, and M.E. Battat, "Parametric Systems Studies of the Aqueous-Based (Slurry) Blanket Concept for Accelerator Transmutation of Waste," *Nucl. Technol.*, **110**, 321 (1995).
5. G.P. Lawrence, R.A. Jameson, and S.O. Schriber, "Accelerator Technology for Los Alamos Nuclear Waste Transmutation and Energy Production Concepts," *Trans. Fusion Technol.,* **20**, 652 (1991).
6. T. Nishida, "TRU Transmutation with High Energy Proton Beam," JAERI-M 90-025, Japan Atomic Energy Institute (1990).
7. J.J. Park, D. Butt, and C.A. Beard, "Review of Liquid Metal Corrosion Issues for Potential Containment Materials for Liquid Lead and Lead-Bismuth Eutectic Spallation Targets as a Neutron Source," *Nucl. Eng. and Design*, **196**, 315 (2000).
8. B.S.P. Shen and M. Merker, *Spallation Nuclear Reactions and Their Applications*, D. Rediel Publishing Company, Boston (1976).

9. M. Steinberg, J.R. Powell, H. Takahashi, P. Grand, and H.J.C. Kouts, "The Linear Acclereator Fuel Enricher Regenerator (LAFER) and Fission Product Transmutor (APEX)," BNL-26951, Brookhaven National Laboratory (1979).
10. T. Nishida, "TRU Transmutation with High Energy Proton Beam," JAERI-M 90-025, Japan Atomic Energy Research Institute (1990).
11. F.D. Michaud, "A Flowing Lead Target for Neutron Production Via Spallation from a High Power Proton Beam," LAUR-92-1252, Los Alamos National Laboratory (1992).
12. S.K. Lee, C.A. Beard, W.B. Wilson, L.L. Daemen, D.J. Liska, L.S. Waters, and M.L. Adams, "Structural Activation Calculations Due to Proton Beam Loss in the APT Accelerator Design," *AIP Conference Proceedings 345, International Conference on Accelerator Driven Transmutation Technologies and Applications*, p. 587-596, Las Vegas, NV (1995).
13. M.G. Houts, C.A. Beard, J.J. Buska, J.W. Davidson, J.W. Durkee, R.T. Perry, and D.I. Poston, "Accelerator driven Molten-Salt Blankets: Physics Issues", *AIP Conference Proceedings 345, International Conference on Accelerator driven Transmutation Technologies and Applications*, p. 564-568, Las Vegas, NV (1995).
14. J.J. Buksa, C.A. Beard, F. Venneri, J.S. Elson, J.J. Park, R.E. Prael, L.S. Waters, and J.W. Davidson, "Conceptual Design of a Thorium Target for Molten Salt Transmutation Systems," *AIP Conference Proceedings 345, International*

Conference on Accelerator driven Transmutation Technologies and Applications, pp. 332-338, July 25-29, Las Vegas, NV (1995).

15. J.J. Park, D. Butt, and C.A. Beard, 2000. "Review of Liquid Metal Corrosion Issues for Potential Containment Materials for Liquid Lead and Lead-Bismuth Eutectic Spallation Targets as a Neutron Source," *Nuclear Engineering and Design*, **196**, 315 (2000).
16. M.S. Wechsler, "Radiation Effects in Materials for Accelerator driven Neutron Technologies," *Journal of Nuclear Materials*, **244**, 177 (1997).
17. T. Mukaiyama, "OMEGA Program in Japan and ADS Development at JAERI," *Proceedings of the 3rd International Conference on Accelerator Driven Technologies and Applications*, June 7-11, Prague, Czech Republic (1999).
18. W. Gudowski, Accelerator driven Transmutation Projects: The Importance of Nuclear Physics Research for Waste Transmutation," *Nuclear Physics*, **A654**, 436 (1999).
19. C. Rubbia, J. A. Rubio, S. Buono, F. Carminati, N. Fietier et al., "Conceptual Design of a Fast Neutron Operated High Power Energy Amplifier," CERN/AT/95-44, European Organization for Nuclear Research (1994).
20. R. Soule and E. Gonzalez-Romero, "The MUSE Experiments for Sub-Critical Neutronics Validation and Proposal for a Computer Benchmark on Simulation of MASCURA Critical and Sub-Critical Experiments," *Proceedings of the 6th*

Information Exchange Meeting on Actinide and Fission Product Partitioning and Transmutation, December 11-13, Madrid, Spain (2000).

21. S. Monti, M. Salvatores, A. d'Angelo, G. Bignan, N. Burgio *et al*., "On the Types and Representativity of Experiments to be Performed in TRADE: TRIGA Accelerator Driven Experiments," TRADE PC:0 TR 001 0, Italian National Agency for New Nuclear Technologies (ENEA) (2003).
22. X-5 Monte Carlo Team, "MCNP-A General Monte Carlo N-Particle Transport Code, Version 5," LA-UR-03-1987, Los Alamos National Laboratory (2003).

APPENDIX A

Bare Target MCNP Input Decks

```
Lead Accelerator Driven Target Design
c
c  ---- Description: ----
c
c        This deck simulates an accelerator driven neutron source.
c        The accelerator source is a 40-MeV electron accelerator.
c        This beam impinges normal to a lead target.  The electrons
c        then create an intense gamma-ray source which in turn
c        generates a photoneutron source. The complete deck requires
c        long run times because only ~1 neutron is created for every
c        100 electrons input.
c
c  --  Cell Cards --
c    - accelerator driven target -
301   0            -301 +304                    imp:n=1 imp:e=0 imp:p=0
302   6 -11.4      -301 +303 -304               imp:n=1 imp:e=1 imp:p=1
303   0            -301      -303               imp:n=1 imp:e=0 imp:p=0
c
c    - universe cells -
9993  0       #301 #302 #303                    imp:n=0 imp:e=0 imp:p=0

c  -- Surface Cards --
c    - accelerator driven target surfaces -
301   cz   +5.400                       $Target Outer Radius
303   pz  -18.00                        $Target Bottom
304   pz   +7.00                        $Target Top

c  -- Data Cards --
c
c    - source definition
mode  n p e
nps   2000
sdef  sur=304 pos=0.0 0.0 +7.0 vec=0 0 1 dir=-1 rad=d1 erg=40.0 par=3
si1   0 0.5
sp1   -21 1
c
c    - tally cards -
f1:n  301
c
c    - material cards -
m6    82206.24c  0.241
      82207.24c  0.221
      82208.25c  0.524      $Lead (density=11.4 g/cc)
c
c  --  End of Deck --
```

```
Tungsten Accelerator Driven Target Design
c
c  --  Cell Cards --
c    - accelerator driven target -
301   0            -301 +304                    imp:n=1 imp:e=0 imp:p=0
302   7 -19.3      -301 +303 -304               imp:n=1 imp:e=1 imp:p=1
303   0            -301      -303               imp:n=1 imp:e=0 imp:p=0
c
c    - universe cells -
9993  0       #301 #302 #303                    imp:n=0 imp:e=0 imp:p=0

c  -- Surface Cards --
c    - accelerator driven target surfaces -
301   cz   +3.000                       $Target Outer Radius
303   pz  -18.00                        $Target Bottom
304   pz   +7.00                        $Target Top

c  -- Data Cards --
c
c    - source definition
mode  n p e
nps   2000
sdef  sur=304 pos=0.0 0.0 +7.0 vec=0 0 1 dir=-1 rad=d1 erg=40.0 par=3
si1   0 0.5
sp1   -21 1
c
c    - tally cards -
f1:n  301
c
c    - material cards - (note: forced photonuclear cross sections)
m7    74182.66c  0.2630
      74183.66c  0.1428
      74184.66c  0.3070
      74186.66c  0.2860     $Tungsten (density=19.3 g/cc)
mpn7  74184 74184 74184 74184
c
c    - physics cards -
c      photon physics card is used to decrease computational time
c      (parameters include: upper limit for photons 2.000 MeV,
c       photons do produce electrons, coherent scattering occurs,
c       biased photonuclear collision sampling, Doppler energy
c       broadening occurs)
phys:p 40.000 0 0 1 0
c
c      electron physics card is used to decrease computational time
c      (parameters include: upper limit for electrons 50 MeV,
c       photons will produce electrons, electrons will produce photons,
c       full bremsstrahlung tabular angular distribution, sampled
c       straggling for electron energy loss, 10 times # of
c       bremsstrahlung photons, x-ray photons produced by electrons,
c       knock-on electrons not produced, photon induced secondary
c       electrons produced, nominal bremsstrahlung production)
phys:e 50   0 0 0 0 10 1 0 1 0
c
c    - cutoff cards -
cut:n  1.0e+17  0.0     0.0   0.0
cut:p  1.0e+17  0.001   0.0   0.0
cut:e  1.0e+17  0.001   0.0   0.0
c
c  --  End of Deck –
```

```
Tungsten-Copper Accelerator Driven Target Design
c  --  Cell Cards --
c    - accelerator driven target -
301   0            -301 +304                    imp:n=1 imp:e=0 imp:p=0
302   7 -16.151    -301 +303 -304               imp:n=1 imp:e=1 imp:p=1
303   0            -301      -303               imp:n=1 imp:e=0 imp:p=0
c
c    - universe cells -
9993  0       #301 #302 #303                    imp:n=0 imp:e=0 imp:p=0

c  -- Surface Cards --
c    - accelerator driven target surfaces -
301   cz   +3.200                       $Target Outer Radius
303   pz  -18.00                        $Target Bottom
304   pz   +7.00                        $Target Top

c  -- Data Cards --
c
c    - source definition
mode  n p e
nps   2000
sdef  sur=304 pos=0.0 0.0 +7.0 vec=0 0 1 dir=-1 rad=d1 erg=40.0 par=3
si1   0 0.5
sp1   -21 1
c
c    - tally cards -
f1:n  301
c
c    - material cards - (forced photonuclear cross sections)
m7    74182.66c            0.18571
      74183.66c            0.10038
      74184.66c            0.21469
      74186.66c            0.19922
      29063.66c            0.20751
      29065.66c            0.09249 $Tungsten-Copper (density=16.1 g/cc)
mpn7 74184 74184 74184 74184 29063 29063
c
c    - physics cards -
c      photon physics card is used to decrease computational time
c      (parameters include: upper limit for photons 2.000 MeV,
c       photons do produce electrons, coherent scattering occurs,
c       biased photonuclear collision sampling, Doppler energy
c       broadening occurs)
phys:p 40.000 0 0 1 0
c
c      electron physics card is used to decrease computational time
c      (parameters include: upper limit for electrons 50 MeV,
c       photons will produce electrons, electrons will produce photons,
c       full bremsstrahlung tabular angular distribution, sampled
c       straggling for electron energy loss, 10 times # of
c       bremsstrahlung photons, x-ray photons produced by electrons,
c       knock-on electrons not produced, photon induced secondary
c       electrons produced, nominal bremsstrahlung production)
phys:e 50   0 0 0 0 10 1 0 1 0
c
c    - cutoff cards -
cut:n  1.0e+17  0.0     0.0   0.0
cut:p  1.0e+17  0.001   0.0   0.0
cut:e  1.0e+17  0.001   0.0   0.0
c
c  --  End of Deck --
```

APPENDIX B

UT-NETL MCNP Input Deck

```
***** UT-TRIGA - Core Model ***** Case:
c
c    Geometry version 3.30
c    Coordinate origin on core axis at core midplane
c    Experiment tubes, empty beam ports, empty RSR
c    TRIGA33d as reference calculation w/rod position TR7; w/det.
c
c    67890123456789012345678901234567890123456789012345678901234567890123456789012345
c    ****0*********0*********0*********0*********0*********0*********0*********0*****
c    Problem geometry cells.
c    ****0*********0*********0*********0*********0*********0*********0*********0*****
c    0         -100  -110  +120                  $Problem region
c              +150  +155                       $Hex core region
c    ****0*********0*********0*********0*********0*********0*********0*********0*****
c    Cells   0 - 199 Basic TRIGA reactor core components
c    ****0*********0*********0*********0*********0*********0*********0*********0*****
c    Reactor core configuration
c    Cells 0 - 9 core grid, plates and holes
  0  1  -1.0   -202  +206                        $Core region
               -231  +232  -233  +234  -235  +236
               -241  +242  -243  +244  -245  +246
         FILL=1                                 $+150  +155
  1  2  -2.7   -206  +207                        $Lower gridplate
               -211  +212  -213  +214  -215  +216
               -221  +222  -223  +224  -225  +226
         FILL=3                                 $+150  +155
  2  2  -2.7   -203  -201  +202                  $Upper gridplate
         FILL=5                                 $+150  +155
c    ****0*********0*********0*********0*********0*********0*********0*********0*****
c    Define configuration U = 1 to 5
  3  1  -1.0   -101  +102  -103                  $Core lattice
               +104  -105  +106        U=1  LAT=2
         FILL=-7:7 -7:7 0:0
       1 1 1 1 1 1 1 1 1 1 1 1 1 1                      $D17 E23
       1 1 1 1 1 1 1   1  06  06  06  06  06   1   1      $E22
       1 1 1 1 1 1  06   8   8   8   8   8   8  06   1
       1 1 1 1 1  06   8   8   8  9(7) 8   8   8  06   1  $E7  E6
       1 1 1 1  06   8   8   8   8   8   8   8   8  06   1  $D5
       1 1 1  06   8   8   8   8   8   8   8   8   8  06   1
       1 1  06   8   8   8   8  17  16   8   8   8   8  06   1
       1   1   8  9(7) 8   8  12  11  15   8   8 7(7)  8   1   1
         1  06   8   8   8   8  13  14   8   8   8   8  06   1 1
           1  06   8   8   8   8   8   8   8   8   8  06   1 1 1
             1  06   8   8   8   8   8   8   8   8  06   1 1 1 1
               1  06   8   8   8  9(7) 8   8   8  06   1 1 1 1 1
                 1  06   8   8   8   8   8   8  06   1 1 1 1 1 1
                   1   1  06  06  06  06  06   1   1 1 1 1 1 1 1
                                1 1 1 1 1 1 1 1 1 1 1 1 1 1 1
c
c    ****0*********0*********0*********0*********0*********0*********0*********0*****
  4  1  -1.0   -205                  U=2
  5  2  -2.7    #4                   U=2
c    ****0*********0*********0*********0*********0*********0*********0*********0*****
  6  2  -2.7   -101  +102  -103                  $Cell lattice
               +104  -105  +106        U=3  LAT=2
         FILL=-7:7 -7:7 0:0
```

```
      3 3 3 3 3 3 3   3  02  02  02  02  02   3   3
      3 3 3 3 3 3  02   2   2   2   2   2   2  02   3
      3 3 3 3 3  02   2   2   2   2   2   2   2  02   3
      3 3 3 3  02   2   2   2 9(7)  2   2   2   2  02   3
      3 3 3  02   2   2   2   2   2   2   2   2   2  02   3
      3 3  02   2   2   2   2   2   2   2   2   2   2  02   3
      3   3   2 9(7)  2   2   2  10   2   2   2  7(7) 2   3   3
        3  02   2   2   2   2   2   2   2   2   2   2  02   3 3
          3  02   2   2   2   2   2   2   2   2   2  02   3 3 3
            3  02   2   2   2 9(7)  2   2   2   2  02   3 3 3 3
              3  02   2   2   2   2   2   2   2  02   3 3 3 3 3
                3  02   2   2   2   2   2   2  02   3 3 3 3 3 3
                  3   3  02  02  02  02  02   3   3 3 3 3 3 3 3
                                3 3 3 3 3 3 3 3 3 3 3 3 3 3 3
c
c    ****0*********0*********0*********0*********0*********0*****
  7  1  -1.0   -200                    U=4
  8  2  -2.7    #7                     U=4
c    ****0*********0*********0*********0*********0*********0*****
  9  2  -2.7   -101  +102  -103                  $Cell lattice
             +104  -105  +106        U=5  LAT=2
         FILL=-7:7 -7:7 0:0
      5 5 5 5 5 5 5 5 5 5 5 5 5 5 5
      5 5 5 5 5 5 5   5  04  04  04  04  04   5   5
      5 5 5 5 5 5  04   4   4   4   4   4   4  04   5
      5 5 5 5 5  04   4   4   4   4   4   4   4  04   5
      5 5 5 5  04   4   4   4 9(7)  4   4   4   4  04   5
      5 5 5  04   4   4   4   4   4   4   4   4   4  04   5
      5 5  04   4   4   4   4   4   4   4   4   4   4  04   5
      5   5   4 9(7)  4   4   4  10   4   4   4  7(7) 4   5   5
        5  04   4   4   4   4   4   4   4   4   4   4  04   5 5
          5  04   4   4   4   4   4   4   4   4   4  04   5 5 5
            5  04   4   4   4 9(7)  4   4   4   4  04   5 5 5 5
              5  04   4   4   4   4   4   4   4   4  04   5 5 5 5 5
                5  04   4   4   4   4   4   4   4  04   5 5 5 5 5 5
                  5   5  04  04  04  04  04   5   5 5 5 5 5 5 5 5 5
                                5 5 5 5 5 5 5 5 5 5 5 5 5 5 5 5 5
c
c    ****0*********0*********0*********0*********0*********0*****
c
c    Reactor core structure
c    Cells 10 - 29 reflector inner core shroud
 10  2  -2.7   -300  +302  -303  +202            $Alignment ring
 11  2  -2.7   -300  -202  +352                  $Alignment ring
              (+231: -232: +241: -242:
               +233: -234: +243: -244:
               +235: -236: +245: -246)
 12  2  -2.7   +305  -306  +307                  $Shroud loadring
              (-311  +312  -321  +322
               -313  +314  -323  +324
               -315  +316  -325  +326)
 13  2  -2.7   -301  -352  +304                  $Alignment ring
              (+331: -332: +341: -342:
               +333: -334: +343: -344:
               +335: -336: +345: -346)
 14  2  -2.7   +231  -331  -233  +236            $Reflector plate
               -352  +306
 15  2  -2.7   -232  +332  +234  -235            $Reflector plate
               -352  +306
 16  2  -2.7   +241  -341  -343  -345            $Reflector, bp3
               -352  +306  +363
 17  2  -2.7   -242  +342  +344  +346            $Reflector plate
               -352  +306
 18  2  -2.7   +233  -333  -331  -343            $Reflector plate
```

```
                -352  +306
 19  2  -2.7    -234  +334  +332  +344            $Reflector plate
                -352  +306
 20  2  -2.7    +235  -335  +332  -345            $Reflector plate
                -352  +306
 21  2  -2.7    -236  +336  -331  +346            $Reflector plate
                -352  +306
 22  2  -2.7    +243  -343  -241  -233            $Reflector plate
                -352  +306
 23  2  -2.7    -244  +344  +242  +234            $Reflector plate
                -352  +306
 24  2  -2.7    +245  -345  -241  -235            $Reflector plate
                -352  +306
 25  2  -2.7    -246  +346  +242  +236            $Reflector plate
                -352  +306
 26  2  -2.7    +241  -363  +364  -360            $Reflector BP3
 27  2  -2.7    -361  +362  -100                  $Reflector BP1&5
c    ****0*********0*********0*********0*********0*********0*********0*****
c    Cells 30 - 39 reflector outer shroud structure
 30  2  -2.7    -355  +361                       $Reflector cylin
                -350  +351  -352  +353
 31  2  -2.7    +355  +363                       $Reflector cylin
                -350  +351  -352  +353
 32  2  -2.7    -370  +371  -372  +373            $Cylinder, top
 33  2  -2.7    -374  -375  +376                  $Cylinder, bot
               (+331: -332: +341: -342:
                +333: -334: +343: -344:
                +335: -336: +345: -346)
 34  2  -2.7    -370  +374  -375  +377            $Rflctr edge rng
 35  2  -2.7    -352  -371  +380  +381            $Rflctor rsrunit
 36  2  -2.7    -380  +300  +381  -382            $Rflctor rsrunit
 37  2  -2.7    -352  +301  -300  +381            $Rflctor rsrunit
 38  1  -1.0    +370  -351  -377  +120            $Edge ring error
c    ****0*********0*********0*********0*********0*********0*********0*****
c    Cells 40 - 49 reflector graphite moderator
 40  4  -2.25     -400  +401  -402  +403          $Rflctr graphite
 41  4  -2.25     -400  -403  +375  -404  +361
                (+411: -412: +421: -422:
                 +413: -414: +423: -424:
                 +415: -416: +425: -426)
                #(-361  +405)                     $Graphite, bp1&5
 42  4  -2.25    (-400  -403  +375  +404  +363
                (+411: -412: +421: -422:
                 +413: -414: +423: -424:
                 +415: -416: +425: -426))
                #(-406 +408) #(-407 +409)         $Graphite, bp3
 43  8 -1.15e-3 (+371 -351 -373 +403)     #40
                                                  $graphite void
                                                  $ <fix this ?>
 44  8 -1.15e-3 (-351  -403  +375  -404  +361
                (+331: -332: +341: -342:
                 +333: -334: +343: -344:
                 +335: -336: +345: -346)) #41    $graphite void
 45  8 -1.15e-3 (-351  -403  +375  +404  +363
                (+331: -332: +341: -342:
                 +333: -334: +343: -344:
                 +335: -336: +345: -346)) #42    $graphite void
 46  8 -1.15e-3  -304  +403  -301
                (+331: -332: +341: -342:
                 +333: -334: +343: -344:
                 +335: -336: +345: -346)         $graphite void
 47  8 -1.15e-3  +301  -371  +403  -381          $graphite void
c    ****0*********0*********0*********0*********0*********0*********0*****
c    Cells 50 - 59 pool coolant water
```

```
c    exterior core water, above and below grid plates
 50  1  -1.0   -203  +201  -110                  $Upper gridplate
 51  1  -1.0   +203  -302  +202  -110            $Upper gridplate
 52  1  -1.0   +302  -300  +303  -110            $Upper gridplate
 53  1  -1.0   -305  -306  +307                  $Lower gridplate
 54  1  -1.0   -307  +120                        $Lower gridplate
              (-311  +312  -321  +322
               -313  +314  -323  +324
               -315  +316  -325  +326)
 55  1  -1.0   -207  +306                        $Lower gridplate
              (-231  +232  -241  +242
               -233  +234  -243  +244
               -235  +236  -245  +246)
 56  1  -1.0   -206  +207                        $Lower gridplate
              (+211: -212: +221: -222:
               +213: -214: +223: -224:
               +215: -216: +225: -226)
              (-231  +232  -241  +242
               -233  +234  -243  +244
               -235  +236  -245  +246)
 57  1  -1.0   -351  +371  +372  -110            $Upper reflector
 58  1  -1.0   -374  -376  +120                  $Lower reflector
              (+311: -312: +321: -322:
               +313: -314: +323: -324:
               +315: -316: +325: -326)
 59  1  -1.0   +306  -376                        $Lower reflector
              (+331: -332: +341: -342:
               +333: -334: +343: -344:
               +335: -336: +345: -346)
              (-311  +312  -321  +322
               -313  +314  -323  +324
               -315  +316  -325  +326)
c    ****0********0********0********0********0********0*****
c    Cells 60 - 69 pool coolant water
c    exterior core water, around reactor core assembly
c 02  8 -1.15e-3    (-406 +408)
c    *TRCL (+35.255  -06.222  -6.985  30 120  90   60  30  90) $BP2
c 04  8 -1.15e-3    (-407 +409)
c    *TRCL (-22.871  +13.216  -6.985  60  30  90  150  60  90) $BP4
950  8 -1.15e-3 -150 +160 -165
     *TRCL (-60.00    00.00   00.00   00  90  90   90  00  90) $NP
951  8 -1.15e-3 -150 +160 -165
     *TRCL ( 57.96   -15.53   00.00   00  90  90   90  00  90) $NPP
952  8 -1.15e-3 -150 +160 -165
     *TRCL ( 42.43    42.43   00.00   00  90  90   90  00  90) $FC
 60  1  -1.0   +350  -355  +361
              (-100  -110  +120) #950 #951       $Beam ports 1&5
 61  1  -1.0   +350  +355  +363
              (-100  -110  +120) #950 #952
             #(-406 +408) #(-407 +409)           $Beam ports 2&4
 62  1  -1.0   -363  +364  +360  -100            $rflctr BP3
 63  1  -1.0   -350  +351  +352  -110            $rflctr cylinder
 64  1  -1.0   -350  +351  -353  +120            $rflctr cylinder
 65  1  -1.0   -370  +374  -377  +120            $rflctr edgering
 66  1  -1.0   +300  -371  +303  -110            $RSR removal
 67  2  -2.7   +370  -351  -375  +377            $edge ring error
 68  2  -2.7   -351  +370  -372  +373            $edge ring error
c    ****0********0********0********0********0********0*****
c    Cells 70 - 79  beam port structure
c    bp 2 & 4 structure
 71  2  -2.7    (-406  +430)
                       +350  +355  -100          $Reflector BP2
 72  2  -2.7    (-407  +440)
                       +350  +355  -100          $Reflector BP4
```

```
c    beam port 3 structure
 73  2  -2.7     +461  -462  -464                $Reflector BP3
 74  2  -2.7     -463  +464  +461  -100          $Reflector BP3
 75  1  -1.0     +241  -364  -461                $Reflector BP3
 76  1  -1.0     +463  -364  +461  -100          $Reflector BP3
c    beam port 1, 3, 5 cavity
 77  8 -1.15e-3  +450  -362  -451                $Reflector BP1
 78  8 -1.15e-3  +462  -464  -453                $Reflector BP3
 79  8 -1.15e-3  -450  -362  +455                $Reflector BP5
c    Cells 80 - 89 beam port cavity
c    beam ports 1, 2, 3, 4 & 5
 81  8 -1.15e-3  +451  -362  -100        VOL=1   $Reflector BP1
 82  8 -1.15e-3 (-430  +408) +350  -100  VOL=1   $Reflector BP2
 83  8 -1.15e-3  +453  -464  -100        VOL=1   $Reflector BP3
 84  8 -1.15e-3 (-440  +409) +350  -100  VOL=1   $Reflector BP4
 85  8 -1.15e-3  -455  -362  -100        VOL=1   $Reflector BP5
c    Cells 90 - 94  rsr unit
c     rotary specimen rack
 90  8 -1.15e-3  +300  -303  +352  -371          $RSR unit
 91  8 -1.15e-3  +300  +304  -352  -380          $RSR unit
 92  8 -1.15e-3  +300  -304  -380  +382          $RSR unit
c    ****0*********0*********0*********0*********0*********0*****
c    Cells 100 - 199 Fill universe for reactor core grid
c                    Basic core components U = 6 to 9
c    ****0*********0*********0*********0*********0*********0*****
c    Cells 100 - 109 graphite reflector elements
100  1 -1.0     #101  #102  #103
                #104  #105  #106        U=6      $element clad
101  2 -2.7     -623  -609              U=6      $lower fitting
102  2 -2.7     -605  -620  +621        U=6      $end closure
103  4 -2.25    -605  -621  +622        U=6      $graphite
104  2 -2.7     -605  -622  +623        U=6      $end closure
105  2 -2.7     +620  -608              U=6      $upper fitting
106  2 -2.7     +605  -607  -620  +623  U=6      $element clad
c    Cells 110 - 119 reactor pulse control
c      transient control rod
c  110  1 -1.0   #(-502  -511  +516)    U=7      $element clad
110  1 -1.0     #111  #112  #113
                #114  #115  #116
                #117                    U=7      $element clad
111  2 -2.7     -500  -510  +511        U=7      $end plug
112  2 -2.7     -500  -511  +512        U=7      $spacer plug
113  6 -2.52    -500  -512  +513        U=7      $absorber
114  2 -2.7     -500  -513  +514        U=7      $spacer plug
115  8 -1.15e-3 -500  -514  +515        U=7      $air follower
116  3 -7.8     -500  -515  +516        U=7      $end plug
117  3 -7.8     +500  -502  -511  +516  U=7      $element clad
c    ****0*********0*********0*********0*********0*********0*****
c    Cells 120 - 129 standard triga fuel element
120  1 -1.0     #121  #122  #123
                #124  #125  #126
                #127  #128  #129        U=8      $element clad
121  3 -7.8     -615  -603              U=8      $lower fitting
122  3 -7.8     -600  -610  +611        U=8      $end closure
123  4 -2.25    -600  -611  +612        U=8      $graphite
124  5 -6.0     -600  -612  +613  +650  U=8      $fuel
125  7 -6.49    -650  -612  +613        U=8      $Zr rod
126  4 -2.25    -600  -613  +614        U=8      $graphite
127  3 -7.8     -600  -614  +615        U=8      $end closure
128  3 -7.8     +610  -604              U=8      $upper fitting
129  3 -7.8     +600  -602  -610  +615  U=8      $element clad
c    ****0*********0*********0*********0*********0*********0*****
c    Cells 130 - 149 fuel follower control rods
c      control rods: reg, shim1 & shim2
```

```
130  1 -1.0   #(-507  -520  +531)       U=9      $element clad
131  3 -7.8     -505  -520  +521        U=9      $end plug
132  8 -1.15e-3 -505  -521  +522        U=9      $top space
133  2 -2.7     -505  -522  +523        U=9      $spacer plug
134  8 -1.15e-3 -505  -523  +524        U=9      $void gap
135  6 -2.52    -505  -524  +525        U=9      $absorber
136  2 -2.7     -505  -525  +526        U=9      $spacer plug
137  8 -1.15e-3 -505  -526  +527        U=9      $void gap
138  5 -6.0     -505  -527  +528  +550  U=9      $fuel follower
139  7 -6.49    -550  -527  +528        U=9      $Zr rod
140  2 -2.7     -505  -528  +529        U=9      $spacer plug
141  8 -1.15e-3 -505  -529  +530        U=9      $bot space
142  3 -7.8     -505  -530  +531        U=9      $end plug
143  3 -7.8     +505  -507  -520  +531  U=9      $element clad
c
c    ****0********0********0********0********0********0*****
c    Cells 200 - 999 Modifications and experiment components
c                    Core experiment modifications U = 10 to 50
c    ****0********0********0********0********0********0*****
c    Cells 200 - 499 core experiments
c     CT tube
200  1 -1.0     +900                     U=10     $CT cell water
201  2 -2.7     -900  +901  -110         U=10     $Center tube
202  1 -1.0     -901   FILL=20 (0 0 0)   U=10     $CT fill water
205  8 -1.15e-3 -905  -907  +909         U=20     $CT sample void
210  1 -1.0     #205                     U=20     $CT sample void
c    ****0********0********0********0********0********0*****
c     PTS system w/o Cd
300  1  -1.0    +910                     U=30     $PTSsystem water
301  2  -2.7    -910  +911  +919  -110   U=30     $PTSsystem outer
302  2  -2.7    -912  +913  +919  -110   U=30     $PTSsystem inner
303  8 -1.15e-3 +912  -914  +916  -110   U=30     $PTS no liner
304  8 -1.15e-3 +912  -914  -916  +919   U=30     $PTS system gap
305  8 -1.15e-3 -911  +914  +919  -110   U=30     $PTS system gap
306  2  -2.7    -913  -917  +918         U=30     $No end shadow
307  8 -1.15e-3 #306  -913  +919  -110   U=30     $PTS system air =2pc
308  2  -2.7    -913  -917  +918         U=30     $Sample capsule
309  2  -2.7    -910  -919  +120         U=30     $end assembly
c     PTS system and Cd
350  1  -1.0    +910                     U=35     $PTSsystem water
351  2  -2.7    -910  +911  +919  -110   U=35     $PTSsystem outer
352  2  -2.7    -912  +913  +919  -110   U=35     $PTSsystem inner
353 10  -8.65   +912  -914  +916  -110   U=35     $PTS Cd liner
354  8 -1.15e-3 +912  -914  -916  +919   U=35     $PTS system gap
355  8 -1.15e-3 -911  +914  +919  -110   U=35     $PTS system gap
356 10  -8.65   -913  -917  +918         U=35     $Cd end shadow
357  8 -1.15e-3 #356  -913  +919  -110   U=35     $PTS system air =2pc
358  2  -2.7    -913  -917  +918         U=35     $sample capsule
359  2  -2.7    -910  -919  +120         U=35     $end assembly
c    ****0********0********0********0********0********0*****
c     GD3 system w/o Cd
400  1  -1.0    +920                     U=40     $T3system water
401  2  -2.7    -920  +921               U=40     $T3system outer
402  2  -2.7    -922  +923               U=40     $T3system inner
403 11 -11.4    +922  -924               U=40     $T3 Pb liner
404  8 -1.15e-3 -921  +924               U=40     $T3 system gap
405  8 -1.15e-3 -923                     U=40
409  8 -1.15e-3 -921 Fill=50 (0 0 0)     U=40     $T3 sample can
410  1  -1.0 -100 fill=40 (+2.17678  +1.0033  0.0) U=41   $D-17
420  1  -1.0 -100 fill=40 ( 0.0      -2.76606 0.0) U=42   $E-22
430  1  -1.0 -100 fill=40 (-2.17678  +1.0033  0.0) U=43   $E-23
450  1  -1.0    +920                     U=45     $T3system water
451  2  -2.7    -920  +921               U=45     $T3system outer
452  2  -2.7    -922  +923               U=45     $T3system inner
```

```
453 10  -8.65   +922  -924              U=45     $T3 Cd liner
454  8 -1.15e-3 -921  +924              U=45     $T3 system gap
455  8 -1.15e-3 -923                    U=45
459  8 -1.15e-3 -921 Fill=50 (0 0 0)    U=45     $T3 sample can
460  1  -1.0 -100 fill=45 (+2.17678  +1.0033  0.0) U=46    $D-17
470  1  -1.0 -100 fill=45 ( 0.0      -2.76606 0.0) U=47    $E-22
480  1  -1.0 -100 fill=45 (-2.17678  +1.0033  0.0) U=48    $E-23
490  8 -1.15e-3 #491  #492  #493  #494  U=50     $CT sample can
491  2  -2.7    -922  +923  -950  +955  U=50     $T3 can cylinder
492  2  -2.7    +922  -924  -950  +955  U=50     $T3 can liner
493  2  -2.7    -923  +950  -951        U=50     $T3 can upper
494  2  -2.7    -923  -955  +956        U=50     $T3 can lower
C
c    ****0*********0*********0*********0*********0*********0*****
c    reactor core modifications
c    central source/ cells
c  501  1  -1.0    -702  +707           U=11  $for central source
502 16  -1.848  -701  -703  +704        U=11  $for central source
503 12  -16.151 -701  -704  +705        U=11  $for central source
504  3  -7.8    -701  -705  +706        U=11  $for central source
505  3  -7.8    -706  +707  -701        U=11  $for central source
506  3  -7.8    +701  -702  -703  +707  U=11  $for central source
507  1  -1.0    #502  #503  #504
                #505  #506              U=11  $for central source
C
C  511  1  -1.0    -711  +707           U=12  $for central source
512 16  -1.848  -711  -703  +704        U=12  $for central source
513 12  -16.151 -711  -704  +705        U=12  $for central source
514  3  -7.8    -711  -705  +706        U=12  $for central source
515  3  -7.8    -706  +707  -711        U=12  $for central source
516  3  -7.8    +711  -712  -703  +707  U=12  $for central source
517  1  -1.0    #512  #513  #514
                #515  #516              U=12  $for central source
C
C  521  1  -1.0    -721  +707           U=13  $for central source
522 16  -1.848  -721  -703  +704        U=13  $for central source
523 12  -16.151 -721  -704  +705        U=13  $for central source
524  3  -7.8    -721  -705  +706        U=13  $for central source
525  3  -7.8    -706  +707  -721        U=13  $for central source
526  3  -7.8    +721  -722  -703  +707  U=13  $for central source
527  1  -1.0    #522  #523  #524
                #525  #526              U=13  $for central source
C
C  531  1  -1.0    -731  +707           U=14  $for central source
532 16  -1.848  -731  -703  +704        U=14  $for central source
533 12  -16.151 -731  -704  +705        U=14  $for central source
534  3  -7.8    -731  -705  +706        U=14  $for central source
535  3  -7.8    -706  +707  -731        U=14  $for central source
536  3  -7.8    +731  -732  -703  +707  U=14  $for central source
537  1  -1.0    #532  #533  #534
                #535  #536              U=14  $for central source
C
C  541  1  -1.0    -741  +707           U=15  $for central source
542 16  -1.848  -741  -703  +704        U=15  $for central source
543 12  -16.151 -741  -704  +705        U=15  $for central source
544  3  -7.8    -741  -705  +706        U=15  $for central source
545  3  -7.8    -706  +707  -741        U=15  $for central source
546  3  -7.8    +741  -742  -703  +707  U=15  $for central source
547  1  -1.0    #542  #543  #544
                #545  #546              U=15  $for central source
C
C  551  1  -1.0    -751  +707           U=16  $for central source
552 16  -1.848  -751  -703  +704        U=16  $for central source
553 12  -16.151 -751  -704  +705        U=16  $for central source
```

```
554  3  -7.8    -751  -705  +706        U=16  $for central source
555  3  -7.8    -706  +707  -751        U=16  $for central source
556  3  -7.8    +751  -752  -703  +707  U=16  $for central source
557  1  -1.0    #552  #553  #554
                #555  #556              U=16  $for central source
C
C  561  1  -1.0    -761  +707           U=17  $for central source
562 16  -1.848  -761  -703  +704        U=17  $for central source
563 12  -16.151 -761  -704  +705        U=17  $for central source
564  3  -7.8    -761  -705  +706        U=17  $for central source
565  3  -7.8    -706  +707  -761        U=17  $for central source
566  3  -7.8    +761  -762  -703  +707  U=17  $for central source
567  1  -1.0    #562  #563  #564
                #565  #566              U=17  $for central source
C
c    ****0********0********0********0********0********0********0*****
c    Cells 500 - 799 beam port experiments
c    Cells 800 - 999 other modifications
c    Core experiment modifications U = 60 to 90
c    ****0********0********0********0********0********0********0*****
c 900  1  -1.0    -150  +160 -165         U=99     $Detector
c 901  1  -1.0 -150 +160 -165  fill=99 (+0.0  +64.0  +0.0) $Detector
1999 0          +100: +110: -120       $Non Problem region
c                   :(-100  -150)
c                   :(-100  -155)
c    ****0********0********0********0********0********0********0*****

c    ****0********0********0********0********0********0********0*****
c    Problem geometry surfaces.
c    ****0********0********0********0********0********0********0*****
c    Define PROBLEM radial domain:
 100     CZ     +75                    $Cylinder
c    hexagonal cell lattice surfaces
 101     PX      +2.17678              $Fuel lattice hex-prism
 102     PX      -2.17678              $Fuel lattice hex-prism
 103     P   +1   1.73205  0  +4.35356 $Fuel lattice hex-prism
 104     P   +1   1.73205  0  -4.35356 $Fuel lattice hex-prism
 105     P   -1   1.73205  0  +4.35356 $Fuel lattice hex-prism
 106     P   -1   1.73205  0  -4.35356 $Fuel lattice hex-prism
c    Define PROBLEM axial domain:
 110     PZ     +75                    $UPPER BOUND
 120     PZ     -75                    $LOWER BOUND
 150     CZ     +5.08                  $Detector Cylinder
 160     PZ     +10                    $Detector Lower
 165     PZ     +30                    $Detector Upper
c 150     P    1  +1.732    0  0        $One-sixth plane
c 155     P    1  -1.732    0  0        $One-sixth plane
c    ****0********0********0********0********0********0********0*****
c
c    reactor core grid plate surfaces
 200     CZ       1.91135    $Grid plate element holes
 201     PZ     +32.3850     $Upper grid plate region
 202     PZ     +30.7975     $Upper grid plate region
 203     CZ      27.6225     $Upper grid plate diameter
 205     CZ       1.5875     $Grid plate coolant holes
 206     PZ     -33.17875    $Lower grid plate region
 207     PZ     -36.35375    $Lower grid plate region
c 208     CZ     +27.6225    $Effective core radius
 211     PX     +26.1216              $Lower grid plate edge
 212     PX     -26.1216              $Lower grid plate edge
 213     P   +1   0.57735  0  +29.0240 $Lower grid plate edge
 214     P   +1   0.57735  0  -29.0240 $Lower grid plate edge
 215     P   -1   0.57735  0  +29.0240 $Lower grid plate edge
 216     P   -1   0.57735  0  -29.0240 $Lower grid plate edge
```

```
 221     PY     +25.1360               $Lower grid plate edge
 222     PY     -25.1360               $Lower grid plate edge
 223     P   +1   1.73205  0  +52.2432 $Lower grid plate edge
 224     P   +1   1.73205  0  -52.2432 $Lower grid plate edge
 225     P   -1   1.73205  0  +52.2432 $Lower grid plate edge
 226     P   -1   1.73205  0  -52.2432 $Lower grid plate edge
 231     PX     +26.6700              $Core shroud inside surface
 232     PX     -26.6700              $Core shroud inside surface
 233     P   +1   0.57735  0  +29.2100 $Core shroud inside surface
 234     P   +1   0.57735  0  -29.2100 $Core shroud inside surface
 235     P   -1   0.57735  0  +29.2100 $Core shroud inside surface
 236     P   -1   0.57735  0  -29.2100 $Core shroud inside surface
 241     PY     +25.4000               $Core shroud inside surface
 242     PY     -25.4000               $Core shroud inside surface
 243     P   +1   1.73205  0  +54.9275 $Core shroud inside surface
 244     P   +1   1.73205  0  -54.9275 $Core shroud inside surface
 245     P   -1   1.73205  0  +54.9275 $Core shroud inside surface
 246     P   -1   1.73205  0  -54.9275 $Core shroud inside surface
c    ****0********0*********0*********0*********0*********0*****
c    core structure surfaces
c    reflector inner shroud
 300     CZ      30.083125             $Grid plate alignment ring
 301     CZ      29.765625             $Grid plate alignment ring
 302     CZ      27.9400               $Grid plate alignment ring
 303     PZ     +33.9725               $Grid plate alignment ring
 304     PZ     +26.3525               $Grid plate alignment ring
c    shroud load ring
 305     CZ      24.7650               $Reflector shroud load ring
 306     PZ     -37.30625              $Reflector shroud load ring
 307     PZ     -39.52875              $Reflector shroud load ring
c
 311     PX     +29.2100               $Reflector shroud support
 312     PX     -29.2100               $Reflector shroud support
 313     P   +1   0.57735  0  +32.385  $Reflector shroud support
 314     P   +1   0.57735  0  -32.385  $Reflector shroud support
 315     P   -1   0.57735  0  +32.385  $Reflector shroud support
 316     P   -1   0.57735  0  -32.385  $Reflector shroud support
 321     PY     +27.9400               $Reflector shroud support
 322     PY  -27.9400                  $Reflector shroud support
 323     P   +1   1.73205  0  +59.3725 $Reflector shroud support
 324     P   +1   1.73205  0  -59.3725 $Reflector shroud support
 325     P   -1   1.73205  0  +59.3725 $Reflector shroud support
 326     P   -1   1.73205  0  -59.3725 $Reflector shroud support
c
 331     PX     +27.3050               $Core shroud plate exterior
 332     PX     -27.3050               $Core shroud plate exterior
 333     P   +1   0.57735  0  +29.8450 $Core shroud plate exterior
 334     P   +1   0.57735  0  -29.8450 $Core shroud plate exterior
 335     P   -1   0.57735  0  +29.8450 $Core shroud plate exterior
 336     P   -1   0.57735  0  -29.8450 $Core shroud plate exterior
 341     PY     +26.0350               $Core shroud plate exterior
 342     PY     -26.0350               $Core shroud plate exterior
 343     P   +1   1.73205  0  +56.5150 $Core shroud plate exterior
 344     P   +1   1.73205  0  -56.5150 $Core shroud plate exterior
 345     P   -1   1.73205  0  +56.5150 $Core shroud plate exterior
 346     P   -1   1.73205  0  -56.5150 $Core shroud plate exterior
c    reflector outer shroud
 350     CZ      54.76875    $Reflector outer shroud
 351     CZ      53.49875    $Reflector outer shroud
 352     PZ     +28.8925     $Outer shroud upper edge
 353     PZ     -32.0675     $Outer shroud lower edge
 355     PY      +0.0        $Core shroud section plane
c    reflector beam ports
 360     PY     +55.5625                $Radial penetrating beam port
```

```
 361     C/X    -35.2552  -6.985   7.62   $Tangential thru beam port
 362     C/X    -35.2552  -6.985   6.9088 $Tangential thru beam port
 363     C/Y      0.0     -6.985  10.160  $Radial penetrating beam port
 364     C/Y      0.0     -6.985   9.525  $Radial penetrating beam port
c
 370     CZ      53.3400     $Reflector top shroud
 371     CZ      37.4650     $Reflector top shroud
 372     PZ     +29.5275     $Reflector top shroud
 373     PZ     +28.2575     $Reflector top shroud
 374     CZ      52.0700     $Reflector inner shroud base
 375     PZ     -27.9400     $Reflector inner shroud base
 376     PZ     -29.5275     $Reflector inner shroud base
 377     PZ     -36.8300     $Reflector shroud edge ring
c    rsr experiment system
 380     CZ      37.1475     $RSR cavity outer ring
 381     PZ      +6.9850     $RSR cavity base
 382     PZ      +7.3025     $RSR cavity base
c    ****0*********0*********0*********0*********0*********0*****
c    graphite reflector surfaces
 400     CZ      53.0225     $Graphite reflector outer radius
 401     CZ      37.7825     $Graphite reflector inner radius
 402     PZ      27.6225     $Graphite reflector upper section
 403     PZ       6.3500     $Graphite reflector section plane
 404     PY     -20.32       $Graphite reflector section plane
 405     PY     -35.2552     $Beam port penetration
c        C/Y      0.0     -6.985  10.160         $Radial penetrating beam port, bp3
c        C/X    -35.2552  -6.985   7.62          $Tangential thru beam port,  bp1&5
 406  2  CY      7.62        $Tangential beam port, bp2
 407  4  CY      7.62        $Radial beam port, bp4
 408  2  PY      0.0         $Tangential beam port, bp2
 409  4  PY      0.0         $Radial beam port, bp4
 411     PX    +27.78125               $Graphite inner surface
 412     PX    -27.78125               $Graphite inner surface
 413     P   +1  0.57735  0  +31.00875  $Graphite inner surface +1
 414     P   +1  0.57735  0  -31.00875  $Graphite inner surface +1
 415     P   -1  0.57735  0  +31.00875  $Graphite inner surface +1
 416     P   -1  0.57735  0  -31.00875  $Graphite inner surface +1
 421     PY    +26.431875            $Graphite inner surface
 422     PY    -26.431875            $Graphite inner surface
 423     P   +1  1.73205  0  +57.30875  $Graphite inner surface +1
 424     P   +1  1.73205  0  -57.30875  $Graphite inner surface +1
 425     P   -1  1.73205  0  +57.30875  $Graphite inner surface +1
 426     P   -1  1.73205  0  -57.30875  $Graphite inner surface +1
c
 430  2  CY      6.9088      $Tangential beam port, bp2
 440  4  CY      6.9088      $Radial beam port, bp4
c
 450     PX      0.0         $BP1&5 origin
c    beam port tally surfaces bp1&5 and bp3
 451     PX     +10.16       $BP1
 453     PY     +40.90       $BP3
 455     PX    -10.16        $BP5
c    pool structure pipe, bp3
 461     PY     +25.600               $Radial penetrating beam port, bp3
 462     PY     +26.235               $Radial penetrating beam port, bp3
 463     C/Y      0.0  -6.985  7.62    $Radial penetrating beam port, bp3
 464     C/Y      0.0  -6.985  6.9088  $Radial penetrating beam port, bp3
c    ****0*********0*********0*********0*********0*********0*****
c    control element surfaces
 500     CZ       1.5113     $Control ELEMENT - absorber surface, radius
c        CZ       1.51638    $Control ELEMENT - clad inner surface
 502     CZ       1.5875     $Control ELEMENT - clad outer surface
 505     CZ       1.6637     $Control ELEMENT - absorber surface, radius
c        CZ       1.6637     $Control ELEMENT - clad inner surface
```

```
 507     CZ       1.7145     $Control ELEMENT - clad outer surface
c
 510     PZ     +33.400      $Control ELEMENT - element plug, end
 511     PZ     +32.765      $Control ELEMENT - magneform plug, upper
 512     PZ     +27.685      $Control ELEMENT - absorber surface,length/2
 513     PZ     -10.415      $Control ELEMENT - absorber surface,length/2
 514     PZ     -12.955      $Control ELEMENT - magneform plug, lower
 515     PZ     -62.1675     $Control ELEMENT - air follower section
 516     PZ     -64.0725     $Control ELEMENT - element plug, end
 c
 520     PZ     +43.560      $Control ELEMENT - element plug, end
 521     PZ     +39.750      $Control ELEMENT - void gap
 522     PZ     +29.2725     $Control ELEMENT - magneform plug, upper
 523     PZ     +28.0025     $Control ELEMENT - void gap
 524     PZ     +27.685      $Control ELEMENT - absorber surface,length/2
 525     PZ     -10.415      $Control ELEMENT - absorber surface,length/2
 526     PZ     -11.685      $Control ELEMENT - magneform plug, lower
 527     PZ     -12.320      $Control ELEMENT - void gap
 528     PZ     -50.420      $Control ELEMENT - fuel follower section
 529     PZ     -52.960      $Control ELEMENT - void gap
 530     PZ     -66.295      $Control ELEMENT - magneform plug, bottom
 531     PZ     -67.565      $Control ELEMENT - element plug, end
c
 550     CZ       0.28575    $Zirconium rod
c
c    ****0*********0*********0*********0*********0*********0*****
c    fuel and moderator element surfaces
 600     CZ       1.816      $FUEL ELEMENT - fuel region surface, radius
c        CZ       1.816      $FUEL ELEMENT - clad inner surface
 602     CZ       1.867      $FUEL ELEMENT - clad outer surface
 603     CZ       1.5306     $FUEL - adapter effective radius, lower
 604     CZ       1.9426     $FUEL - adapter effective radius, upper
 605     CZ       1.816      $Graphite ELEMENT - element surface, radius
c        CZ       1.816      $Graphite ELEMENT - clad inner surface
 607     CZ       1.867      $Graphite ELEMENT - clad outer surface
 608     CZ       1.9426     $Graphite - adapter effective radius, upper
 609     CZ       1.5306     $Graphite - adapter effective radius, lower
c
 610     PZ     +28.5877     $FUEL ELEMENT - element end region, upper
 611     PZ     +27.7368     $FUEL ELEMENT - graphite end region, upper
 612     PZ     +19.05       $FUEL ELEMENT - fuel surface, length/2
 613     PZ     -19.05       $FUEL ELEMENT - fuel surface, length/2
 614     PZ     -27.7368     $FUEL ELEMENT - graphite end region, lower
 615     PZ     -28.5877     $FUEL ELEMENT - element end region, lower
c
 620     PZ     +28.5877     $Graphite ELEMENT - element end, upper
 621     PZ     +27.7368     $Graphite ELEMENT - graphite end, upper
 622     PZ     -27.7368     $Graphite ELEMENT - graphite end, lower
 623     PZ     -28.5877     $Graphite ELEMENT - element end, lower
c
 650     CZ       0.28575          $Zirconium rod
c    ****0*********0*********0*********0*********0*********0*****
c    reactor core modifications
c    central source
 701     cz     +4.206
 702     cz     +4.780
c
 703     pz     +10.001
 704     pz     +10.000
 705     pz     -15.000
 706     pz     -19.000
 707     pz     -19.574
c
 C  703     pz     +28.5877
```

```
 C  704     pz     +28.5867
 C  705     pz     -03.5867
 C  706     pz     -28.0137
 C  707     pz     -28.5877
C
 711     c/z    +4.35356  +0.0000000  +4.206
 712     c/z    +4.35356  +0.0000000  +4.780
C
 721     c/z    +2.17678  -3.7702936  +4.206
 722     c/z    +2.17678  -3.7702936  +4.780
C
 731     c/z    -2.17678  -3.7702936  +4.206
 732     c/z    -2.17678  -3.7702936  +4.780
C
 741     c/z    -4.35356  +0.0000000  +4.206
 742     c/z    -4.35356  +0.0000000  +4.780
C
 751     c/z    -2.17678  +3.7702936  +4.206
 752     c/z    -2.17678  +3.7702936  +4.780
C
 761     c/z    +2.17678  +3.7702936  +4.206
 762     c/z    +2.17678  +3.7702936  +4.780
c
c    ****0*********0*********0*********0*********0*********0*********0*****
c    reactor core modifications, surfaces
c    center tube irradiations
 900     CZ       1.905               $ Center tube outer radius
 901     CZ       1.69418             $ Center tube inner radius
 905     CZ       1.5                 $Sample radius
 907     PZ      +0.5                 $Sample length
 909     PZ      -0.5                 $Sample length
c    1-element experiment; PTS tube with/out Cd
c    reference to lower grid plate -33.17875
 910     CZ      +1.74625             $Al transport tube outer radius
 911     CZ      +1.53543             $Al transport tube inner radius
 912     CZ      +1.11125             $Al sample tube outer radius
 913     CZ      +0.86995             $Al sample tube inner radius
 914     CZ      +1.16205             $Cd two layer liner
c 915     PZ      -2.07645             $PTS sample stop
 916     PZ     -18.89125             $Cd absorber end
 917     PZ     -21.1264591           $Cd absorber disk, upper edge
 918     PZ     -21.17725             $Cd absorber disk, lower edge
 919     PZ     -30.32125             $PTS bottom section
c    3-element experiment; tube with Cd or Pb
c    reference to lower grid plate -33.17875
 920     CZ      +2.38125             $Al can outer radius
 921     CZ      +2.2225              $Al can inner radius
 922     CZ      +2.06375             $Al sleeve outer radius
 923     CZ      +1.93929             $Al sleeve inner radius
 924     CZ      +2.16535             $Cd liner outer radius
c 930     CZ      +0.47625             $Al structure rod
c 940     PZ      -30.xxxx             $Al bearing section
 950     PZ      +2.54                $Al upper end cap
 951     PZ      +2.5908              $Al upper end cap
 955     PZ      -2.54                $Al lower end cap
 956     PZ      -2.5908              $Al lower end cap
c    ****0*********0*********0*********0*********0*********0*********0*****

c    ****0*********0*********0*********0*********0*********0*********0*****
c    Append problem data.
c    ****0*********0*********0*********0*********0*********0*********0*****
c
c    Transformations for beam tube locations:
c
```

```
c Thru port, small
  *TR1  0.0      -35.255  -6.985  00  90  90   90  00  90  $BP1
c Tang port, small
  *TR2  +35.255  -06.222  -6.985  30 120  90   60  30  90  $BP2
c Radial port, large
  *TR3  0.0      +25.600  -6.985  00  90  90   90  00  90  $BP3
c Radial port, small
  *TR4  -22.871  +13.216  -6.985  60  30  90  150  60  90  $BP4
c Thru port, large
  *TR5  0.0      -35.255  -6.985  00  90  90   90  00  90  $BP5
c
c    Transformations for control rod positions:
c
  TR6  0  0  00.00     1 0 0  0 1 0    $(000 u) shutdown condition
  TR7  0  0  20.83594  1 0 0  0 1 0    $(525 u) low power critical
  TR8  0  0  27.78125  1 0 0  0 1 0    $(700 u) design high power
  TR9  0  0  38.10     1 0 0  0 1 0    $(960 u) full-out condition
c
c    ****0********0********0********0********0********0*****
c
mode n p e
nps  4000
rand seed=1
sdef  sur=704 pos=0.0 0.0 +10.000 vec=0 0 1 dir=-1 rad=d1
      erg=40.0 par=3
si1   0 0.5
sp1   -21 1
phys:p 1000 0 0 1 0
phys:e 50   0 0 0 0 10 1 0 1 0
cut:n  1e+33   0.0    0.0  0.0
cut:p  1e+33   0.001  0.0  0.0
cut:e  1e+33   0.001  0.0  0.0
c
c    Materials for reactor components
M1    1001.66c     .66667
      8016.66c     .33333              $H2O, coolant & moderator
MT1   lwtr.01t                         $300K
mpn1  0 0
M2   13027.92c   -0.9685
     26000.50c   -0.0070
     29000.50c   -0.0025
     14000.60c   -0.0060
     12000.66c   -0.0110
     24000.50c   -0.0035
     25055.66c   -0.0015                $AL structure type 6061
mpn2 0 0 0 0 0 0 0
c     22000.      -0.0015               $titanium: 0.15
c     30000.      -0.0025               $zinc: 0.25
M3   26000.50c   -0.6785
      6000.66c   -0.0080
     14000.60c   -0.0100
     24000.50c   -0.1800
     28000.50c   -0.0980
     25055.66c   -0.0180
     15031.66c   -0.0045
     16000.66c   -0.0030               $SS structure type 304
mpn3  0 0 0 0 0 0 0 0
M4    6000.66c    1.0                  $C graphite
MT4   grph.01t                         $300K
mpn4  0
M5   40000.66c   -0.8991045
      1001.66c   -0.0158955
     92238.66c   -0.068170
     92235.66c   -0.016830            $Fresh U-ZrH Fuel
```

```
MT5   zr/h.01t
      h/zr.01t
mpn5  0 0 0 0
M6    5010.66c     .1584               $B4C
      5011.66c     .6416               $B4C
      6000.66c     .2                  $carbon
mpn6  0 0 0
M7   40000.66c    1.0                  $Zr Rod
mpn7  0
M8    8016.66c   -0.23                  $air
      7014.66c   -0.77
mpn8  0 0
M09   2004.66c    1.0                  $helium
mpn9  0
M11  82000.50c   -1.0                  $Pb neutron absorber liner
mpn11 0
c  m12   82206.24c         0.241
c        82207.24c         0.221
c        82208.25c         0.538
m12   74182.66c            0.18571
      74183.66c            0.10038
      74184.66c            0.21469
      74186.66c            0.19922
      29063.66c            0.20751
      29065.66c            0.09249
Mpn12 74184
      74184
      74184
      74184
      29063
      29063
m13   26056.60c             1
mpn13 0
m14   13027.66c             1
mpn14 0
m15   1001.66c          0.111
      8016.66c          0.889
mpn15 0 0
M10  48000.50c   -1.0                  $Cd neutron absorber liner
mpn10 0
m16   4009.66c              1
mpn16 0
c    ****0*********0*********0*********0*********0*********0*****
c
IMP:N   1 173r 1 1 4r 1 1 4r 1 1 4r 1 1 4r 1 1 4r 1 1 4r 1 1 3r 0
IMP:P   1 173r 1 1 4r 1 1 4r 1 1 4r 1 1 4r 1 1 4r 1 1 4r 1 1 3r 0
IMP:E   0 173r 1 0 4r 1 0 4r 1 0 4r 1 0 4r 1 0 4r 1 0 4r 1 0 3r 0
f7:n    124
f17:n   (124<U=8)
f6:n    124
f26:n   (124<U=8)
f16:p    124
f36:p   (124<U=8)
c
c  MODE     N
c  IMP:N    1         214r      0
c    Criticality calculation
c  kcode   10000      0.98         100       200
c  ksrc    3.5       7         13.06068
```

APPENDIX C

TTS MCNP Input Deck

```
Initial TTS Core Design
c
c
c  ---- Description: ----
c
c        This deck simulates a full-core subcritical design using
c        TRIGA reactor fuel and an accelerator driven neutron source.
c        The accelerator source is a 40-MeV electron accelerator.
c        This beam impinges normal to a lead target in the center of
c        the core.  The electrons then create an intense gamma-ray
c        source which in turn generates a photoneutron source. The
c        complete deck requires long run times because only ~1 neutron
c        is created for every 100 electrons input.
c
c
c 34567890123456789012345678901234567890123456789012345678901234567890123456789012
c
c  --  Cell Cards --
c
c    - standard TRIGA fuel element -
101   1 -6.49      -101 +105 -106           u=1 imp:n=2 imp:e=0 imp:p=1
102   8 -6.00 +101 -102 +105 -106           u=1 imp:n=2 imp:e=0 imp:p=1
103   3 -2.25      -102 +104 -105           u=1 imp:n=2 imp:e=0 imp:p=1
104   3 -2.25      -102 +106 -107           u=1 imp:n=2 imp:e=0 imp:p=1
105   4 -7.80      -103      -104           u=1 imp:n=2 imp:e=0 imp:p=1
106   4 -7.80 +102 -103 +104 -107           u=1 imp:n=2 imp:e=0 imp:p=1
107   4 -7.80      -103      +107           u=1 imp:n=2 imp:e=0 imp:p=1
108   5 -1.00 +103                          u=1 imp:n=2 imp:e=0 imp:p=1
c
c    - water hole -
201   5 -1.00       -201                    u=2 imp:n=2 imp:e=0 imp:p=1
202   5 -1.00 +201                          u=2 imp:n=2 imp:e=0 imp:p=1
c
c    - accelerator driven target -
301   0             -301 +304               u=3 imp:n=1 imp:e=0 imp:p=1
302   6 -11.4       -301 +303 -304          u=3 imp:n=1 imp:e=1 imp:p=1
303   4 -7.80       -301      -303          u=3 imp:n=1 imp:e=0 imp:p=1
304   4 -7.80 +301 -302                     u=3 imp:n=1 imp:e=0 imp:p=1
305   5 -1.00 +302                          u=3 imp:n=1 imp:e=0 imp:p=1
c
401   0             -401 +304               u=4 imp:n=1 imp:e=0 imp:p=1
402   6 -11.4       -401 +303 -304          u=4 imp:n=1 imp:e=1 imp:p=1
403   4 -7.80       -401      -303          u=4 imp:n=1 imp:e=0 imp:p=1
404   4 -7.80 +401 -402                     u=4 imp:n=1 imp:e=0 imp:p=1
405   5 -1.00 +402                          u=4 imp:n=1 imp:e=0 imp:p=1
c
501   0             -501 +304               u=5 imp:n=1 imp:e=0 imp:p=1
502   6 -11.4       -501 +303 -304          u=5 imp:n=1 imp:e=1 imp:p=1
503   4 -7.80       -501      -303          u=5 imp:n=1 imp:e=0 imp:p=1
504   4 -7.80 +501 -502                     u=5 imp:n=1 imp:e=0 imp:p=1
505   5 -1.00 +502                          u=5 imp:n=1 imp:e=0 imp:p=1
c
601   0             -601 +304               u=6 imp:n=1 imp:e=0 imp:p=1
602   6 -11.4       -601 +303 -304          u=6 imp:n=1 imp:e=1 imp:p=1
603   4 -7.80       -601      -303          u=6 imp:n=1 imp:e=0 imp:p=1
604   4 -7.80 +601 -602                     u=6 imp:n=1 imp:e=0 imp:p=1
```

```
605   5 -1.00 +602                              u=6 imp:n=1 imp:e=0 imp:p=1
c
701   0            -701 +304                    u=7 imp:n=1 imp:e=0 imp:p=1
702   6 -11.4      -701 +303 -304               u=7 imp:n=1 imp:e=1 imp:p=1
703   4 -7.80      -701      -303               u=7 imp:n=1 imp:e=0 imp:p=1
704   4 -7.80 +701 -702                         u=7 imp:n=1 imp:e=0 imp:p=1
705   5 -1.00 +702                              u=7 imp:n=1 imp:e=0 imp:p=1
c
801   0            -801 +304                    u=8 imp:n=1 imp:e=0 imp:p=1
802   6 -11.4      -801 +303 -304               u=8 imp:n=1 imp:e=1 imp:p=1
803   4 -7.80      -801      -303               u=8 imp:n=1 imp:e=0 imp:p=1
804   4 -7.80 +801 -802                         u=8 imp:n=1 imp:e=0 imp:p=1
805   5 -1.00 +802                              u=8 imp:n=1 imp:e=0 imp:p=1
c
901   0            -901 +304                    u=9 imp:n=1 imp:e=0 imp:p=1
902   6 -11.4      -901 +303 -304               u=9 imp:n=1 imp:e=1 imp:p=1
903   4 -7.80      -901      -303               u=9 imp:n=1 imp:e=0 imp:p=1
904   4 -7.80 +901 -902                         u=9 imp:n=1 imp:e=0 imp:p=1
905   5 -1.00 +902                              u=9 imp:n=1 imp:e=0 imp:p=1
c
c
c    - core lattice cells (102 fuel rods in lattice) -
81    0       -84  +81  -83  +86  -82  +85  u=20 imp:n=2 imp:e=1 imp:p=1
         lat=2 fill=-8:8 -8:8 0:0
      2 2 2 2 2 2 2 2 2   2   2   2   2   2   2   2   2
      2 2 2 2 2 2 2 2   2   2   1   1   1   1   2   2   2
      2 2 2 2 2 2 2   2   1   1   1   1   1   1   1   2   2
      2 2 2 2 2 2   1   1   1   1   1   1   1   9   8   1   1   2
      2 2 2 2 2   1   1   1   1   1   1   1   4   3   7   1   1   2
      2 2 2 2   1   1   1   1   1   1   1   5   6   1   1   1   2
      2 2 2   1   1   1   1   1   1   1   1   1   1   1   1   1   2
      2 2   2   1   9   8   1   1   9   8   1   1   1   1   1   2   2
      2   2   1   4   3   7   1   4   3   7   1   1   1   1   1   2   2
        2   2   1   5   6   1   1   5   6   1   1   1   1   1   2   2 2
          2   1   1   1   1   1   1   1   1   1   1   1   1   1   2 2 2
            2   1   1   1   1   1   1   1   9   8   1   1   1   2 2 2 2
              2   1   1   1   1   1   1   4   3   7   1   1   2 2 2 2 2
                2   1   1   1   1   1   1   5   6   1   1   2 2 2 2 2 2
                  2   2   1   1   1   1   1   1   1   2   2 2 2 2 2 2 2
                    2   2   2   1   1   1   1   2   2   2 2 2 2 2 2 2 2
                      2   2   2   2   2   2   2   2   2 2 2 2 2 2 2 2 2
c
c    - full core cells -
91    0            -90  +93  -94         fill=20 imp:n=2 imp:e=1 imp:p=1
92    5 -1.0  +90  -91  +93  -94                 imp:n=2 imp:e=0 imp:p=1
93    5 -1.0       -91  +92  -93                 imp:n=2 imp:e=0 imp:p=1
94    5 -1.0       -91  +94  -95                 imp:n=2 imp:e=0 imp:p=1
c
c    - universe cells -
9991  0            -91       -92                 imp:n=0 imp:e=0 imp:p=0
9992  0            -91  +95                      imp:n=0 imp:e=0 imp:p=0
9993  0       +91                                imp:n=0 imp:e=0 imp:p=0

c
c  -- Surface Cards --
c
c    - fuel element surfaces
c
c        (This fuel element lattice uses standard TRIGA fuel dimensions)
c
101   cz   +0.2857                      $Zirconium Rod Outer Radius
102   cz   +1.8160                      $Fuel/Graphite Outer Radius
103   cz   +1.8670                      $Clad Outer Radius
104   pz  -27.7368                      $Graphite Bottom
```

```
105   pz  -19.0500                     $Fuel Bottom
106   pz  +19.0500                     $Fuel Top
107   pz  +27.2368                     $Graphite Top
c
c    - water hole surfaces -
201   cz  +10.0
c
c    - accelerator driven target surfaces -
c
c       (This target uses a standard steel pipe with an OD of 4.000" and
c       an ID of 3.548".  This is filled with lead. The beam window
c       has been ignored.  The target fills u=3,4,5,6,7,8, and 9 in the
c       core lattice. If pin-to-pin pitch is changed surfaces 401-902
c       must be changed.)
c
301   cz   +4.506                      $Target Outer Radius
302   cz   +5.080                      $Clad Outer Radius
303   pz  -18.00                       $Target Bottom
304   pz   +7.00                       $Target Top
c
401   c/z  +4.4000 +0.00000 +4.506
402   c/z  +4.4000 +0.00000 +5.080
c
501   c/z  +2.2000 -3.81051 +4.506
502   c/z  +2.2000 -3.81051 +5.080
c
601   c/z  -2.2000 -3.81051 +4.506
602   c/z  -2.2000 -3.81051 +5.080
c
701   c/z  -4.4000 +0.00000 +4.506
702   c/z  -4.4000 +0.00000 +5.080
c
801   c/z  -2.2000 +3.81051 +4.506
802   c/z  -2.2000 +3.81051 +5.080
c
901   c/z  +2.2000 +3.81051 +4.506
902   c/z  +2.2000 +3.81051 +5.080
c
c    - core lattice element surfaces -
c
c       (The pin-to-pin lattice spacing is 4.4 cm)
c
81    px   -2.2
82    p    -0.57735 +1.0 +0.0 +2.54034
83    p    +0.57735 +1.0 +0.0 +2.54034
84    px   +2.2
85    p    -0.57735 +1.0 +0.0 -2.54034
86    p    +0.57735 +1.0 +0.0 -2.54034
c
c    - core surfaces -
90    cz  +30.8                        $Outer Core Radius
91    cz  +60.0                        $Outer Radial Water Reflector
92    pz  -40.0                        $Bottom of Axial Water Reflector
93    pz  -28.5877                     $Bottom of Core
94    pz  +28.5877                     $Top of Core
95    pz  +40.0                        $Top of Axial Water Reflector

c
c  -- Data Cards --
c
c
c    - source definition
c
c       (There are two sources here. One is a criticality source using a
```

```
c        single initial source position.  The other is a electron beam
c        source positioned on the central target. To move the electron
c        beam source to the other targets we simply change the position
c        parameter on sdef. The electron beam source takes a very long
c        time to run.)
c
c mode  n
c kcode 20000 1.0 50 450
c ksrc   +9.708 +0.0    +0.0
c        -4.854 +8.4073 +0.0
c        -4.854 -8.4073 +0.0
c
rand  seed=1
mode  n p e
nps   4000
sdef  sur=304 pos=-17.5 0.0 0.0 vec=0 0 1 dir=-1 rad=d1 erg=40.0 par=3
si1   0 0.5
sp1   -21 1
phys:p 1000 0 0 1 0
phys:e 50   0 0 0 0 10 1 0 1 0
cut:n  1e+33   0.0    0.0  0.0
cut:p  1e+33   0.001  0.0  0.0
cut:e  1e+33   0.001  0.0  0.0
c
c
c    - tally cards -
f7:n  302                $Fission Energy Deposition in the target
f17:n  (302<u=3)
f27:n  (402<u=4)
f37:n  (502<u=5)
f47:n  (602<u=6)
f57:n  (702<u=7)
f67:n  (802<u=8)
f77:n  (902<u=9)
f6:n  302                $Energy Deposition in the target from Neutrons
f16:n  (302<u=3)
f26:n  (402<u=4)
f36:n  (502<u=5)
f46:n  (602<u=6)
f56:n  (702<u=7)
f66:n  (802<u=8)
f76:n  (902<u=9)
f86:p  302                $Energy Deposition in the target from Photons
f96:p   (302<u=3)
f106:p  (402<u=4)
f116:p  (502<u=5)
f126:p  (602<u=6)
f136:p  (702<u=7)
f146:p  (802<u=8)
f156:p  (902<u=9)
f87:n   102              $Fission Energy Deposition in the Fuel
f97:n  (102<u=1)
f166:n  102              $Energy Deposition in the Fuel from Neutrons
f176:n  (102<u=1)
f186:p  102              $Energy Deposition in the Fuel from Photons
f196:p  (102<u=1)
c
c    - material cards - (note: photonuclear turned off for all except Pb)
m1    40000.66c +1.0        $Pure Zirconium (density=6.49 g/cc)
mpn1      0
m2    40000.66c -0.8991045
       1001.66c -0.0158955
      92238.66c -0.0681700
      92235.66c -0.0168300  $Fresh U-ZrH Fuel (density=6.00 g/cc)
```

```
mpn2      0 0 0 0
m3     6000.66c +1.0        $Pure Graphite (density=2.25 g/cc)
mpn3      0
m4    26000.50c -0.6785
       6000.66c -0.0080
      14000.60c -0.0100
      24000.50c -0.1800
      28000.50c -0.0980
      25055.66c -0.0180
      15031.66c -0.0045
      16000.66c -0.0030     $SS-304 (density=7.80 g/cc)
mpn4      0 0 0 0 0 0 0 0
m5     1001.66c +0.6666667
       8016.66c +0.3333333  $Light Water(density=1.00 g/cc)
mpn5      0 0
mt5    lwtr.01t             $300K
m6    82206.24c  0.241
      82207.24c  0.221
      82208.25c  0.524      $Lead (density=11.4 g/cc)
m7    13027.92c -0.9685
      26000.50c -0.0070
      29000.50c -0.0025
      14000.60c -0.0060
      12000.66c -0.0110
      24000.50c -0.0035
      25055.66c -0.0015     $Aluminum type 6061 (density=2.70 g/cc)
mpn7      0 0 0 0 0 0 0
m8    40000.66c -0.8991045
       1001.66c -0.0158955
      92238.66c -0.0681700
      92235.66c -0.0122300
      26056.66c -0.0046000  $Spent U-ZrH Fuel (1/3rd burnt)
mpn8      0 0 0 0 0
c
c
c 3456789012345678901234567890123456789012345678901234567890123456789012
c
c  --  End of Deck --
```

VITA

TARAKNATH WODDI VENKAT KRISHNA was born on September 03, 1973 to PATTABHIRAM AND BASANTI PATRA in Berhampur (city), Orissa (state), India. He graduated from College of Engineering and Technology of Orissa University of Agriculture and Technology, received his Bachelor of Technology in Instrumentation & Electronics in July 1996. And is married to a beautiful girl named Divya Epari and his permanent address is Flat # 19, Joytsna Apartments, Sasthri Nagar, UNIT – IV, Bhubanewar, ORISSA, INDIA, Pin – 751001.